doi:10.26443/seismica.v5i1.1959

Small earthquake moment magnitude and implications for frequency–magnitude scaling of injection induced earthquakes of the Raton Basin

Andres Felipe Peña Castro *[1], **Brandon Schmandt** [2], **Margaret Glasgow** [3], **Mohammadreza Jamalreyhani** [4,5], **Ruijia Wang** [4], **Elizabeth S. Cochran** [6]

[1]Department of Earth and Planetary Sciences, University of New Mexico, Albuquerque, New Mexico, U.S.A., [2]Department of Earth, Environmental, and Planetary Sciences, Rice University, Houston, Texas, U.S.A, [3]U.S. Geological Survey, California Volcano Observatory, Moffett Field, California, U.S.A, [4]Department of Earth and Space Sciences, Southern University of Science and Technology, Shenzhen, Guangdong, People's Republic of China, [5]School of Earth and Space Sciences, University of Science and Technology of China., [6]U.S. Geological Survey, Earthquake Science Center, Pasadena, California, U.S.A

Author contributions: *Conceptualization*: Andres Felipe Peña Castro, Brandon Schmandt, Margaret Glasgow, Mohammadreza Jamalreyhani, Ruijia Wang, Elizabeth S. Cochran. *Methodology*: Andres Felipe Peña Castro. *Formal Analysis*: Andres Felipe Peña Castro. *Writing - Original draft*: Andres Felipe Peña Castro, Brandon Schmandt,. *Writing - Review & Editing*: Andres Felipe Peña Castro, Brandon Schmandt, Margaret Glasgow, Mohammadreza Jamalreyhani, Ruijia Wang, Elizabeth S. Cochran. *Project administration*: Brandon Schmandt. *Funding acquisition*: Brandon Schmandt.

Abstract Accurate estimation of earthquake source parameters—such as moment magnitudes, corner frequencies, and stress drops—is essential for improving seismic hazard assessments and understanding earthquake physics. In this study, moment magnitudes (M_W) are calculated for 31,581 earthquakes associated with wastewater injection in the Raton Basin (located along the border between northern New Mexico and southern Colorado) between 2016 and 2024 using radiative transfer theory to fit coda decay envelopes. Our results show that it is feasible to estimate moment magnitudes down to $M_W \sim 1$ with coda envelopes from a small local monitoring network. Significant differences were found between M_W and local magnitudes (M_L) for small earthquakes ($M < 3.0$). A linear relationship was optimized to convert M_L to M_W: $M_W = 0.7M_L + 0.96$ and $M_W = 0.73M_L + 0.99$ (for the events reported by the U.S. Geological Survey), which can be applied in future studies of Raton Basin seismicity. We find that b-values calculated employing different methods and using M_L are approximately 1.0, while those using M_W range from 1.2 to 1.4. A larger estimate of the b-value could influence interpretations of the statistical behavior of earthquakes associated with injection and consequently seismic hazard assessments based on a magnitude–frequency distribution. The potential differences between local versus moment magnitude-based earthquake statistics should be considered in other seismically active regions.

Production Editor: Yen Joe Tan
Handling Editor: Giuseppe Petrillo
Copy & Layout Editor: Tara Nye

Received: August 17, 2025
Accepted: February 3, 2026
Published: February 24, 2026

1 Introduction

Earthquake magnitude (M) is a quantitative measurement of earthquake size. Different magnitude types have been developed based on different principles: duration magnitude, local magnitude, moment magnitude, surface wave magnitude, among others. Magnitude metrics are important aspects of seismology since: (i) they inform the public about the event size, (ii) they are used to derive other source properties including stress drop and radiated seismic energy (Prieto et al., 2004), (iii) they help constrain frequency-magnitude statistics that may provide insight into earthquake source processes (Bachmann et al., 2012), and (iv) they are sometimes used for regulatory decisions such as traffic light protocols for induced seismicity (Verdon and Bommer, 2020).

The most commonly reported magnitude type for the past several decades, and even for modern machine learning-based earthquake catalogs, (e.g., Tan et al., 2021; Liu et al., 2022; Gong et al., 2023) is the local magnitude (M_L; Richter, 1935), which only requires a source-receiver distance and a measurement of the peak amplitude of a filtered seismogram. The local magnitude scale was developed based on short-period seismic instruments for events located in California. With the increasing availability of seismic array data covering a range of distances, Hutton and Boore (1987) and Bakun and Joyner (1984) observed that distant stations tended to overestimate M_L, whereas closer stations tended to underestimate M_L compared to intermediate distance stations ($\approx$ 100 km). To accommodate such distance-dependence, Hutton and Boore (1987) and Bakun and Joyner (1984) proposed the addition of specific terms, estimated using regression analysis techniques (Joyner et al., 1981), to the original formulation including: individual station corrections, a geometric spreading coefficient, and an attenuation coefficient.

Since then, different studies have developed local magnitude formulas that account for the local attenu-

*Corresponding author: andresfpenacastro@gmail.com

ation properties of a particular region (e.g., Di Bona, 2016; Ottemoller and Sargeant, 2013; Yenier, 2017; Kim and Park, 2005; Chovanová and Kristek, 2018). M_L derived from regionally-calibrated formulas are reported by many national or local seismic monitoring agencies. Despite such widespread use of M_L, the consistency and accuracy of M_L are challenged by large variations in estimates (Deichmann, 2006) from station to station, influences of radiation pattern and rupture directivity, and spatially variable attenuation structure. In addition, Deichmann (2006) highlights that M_L might not be physically meaningful for small events, as the systematic and random errors in its determination are likely greater than its variability relative to moment magnitude estimates.

Moment magnitude (M_W; Hanks and Kanamori, 1979; Shearer, 2019) or potency magnitude (M_P; Ben-Zion, 2001; Trugman and Ben-Zion, 2024) offers more physics based measurements of earthquake sizes, both relying on the estimation of the seismic moment (M_0). Seismic moment can be estimated by waveform inversions using Green's functions from simple reference models or by measuring the low-frequency spectral plateau of seismograms (Ω_0). Moment magnitudes are commonly reported for moderate-to-large earthquakes ($M > 4$) but less often reported for smaller earthquakes ($M < 3$; Alvizuri and Tape, 2016) due to the limited signal-to-noise ratio at low frequencies (i.e., < 1 Hz) necessary for waveform inversions that involve full moment tensor analysis.

For smaller earthquakes where full moment tensor inversions are often unfeasible, other techniques have been developed to estimate M_W or other source parameters. These techniques involve measurement of Ω_0 including individual spectral fitting of body waves, spectral decomposition, generalized inversion techniques (Shible et al., 2022; Morasca et al., 2025), or coda wave analysis (Mayeda et al., 2003; Eulenfeld et al., 2021), amongst others. Such techniques have been applied successfully to both natural and induced sequences, such as the 2016–2017 Central Italy sequence (Morasca et al., 2022; Kemna et al., 2021), the 2019 Ridgecrest (Trugman, 2020; Mayeda et al., 2024) earthquake sequences, as well as seismicity associated with wastewater injection (Kemna et al., 2020; Shelly et al., 2021), hydraulic fracturing (Wang et al., 2020a), and enhanced geothermal systems (Eulenfeld et al., 2023). These studies provide essential insights into earthquake size, stress-drop scaling, source heterogeneity, and rupture complexity. Understanding these source parameters (including M_W) is a critical step toward improving hazard assessments and mitigating the risks posed by induced seismicity.

Induced earthquakes started to increase in the central United States around 2009 as a consequence of wastewater injection from oil and gas operations (Ellsworth, 2013). One of the regions where this increase in seismicity was first observed is the Raton Basin, located along the Colorado–New Mexico border. Prior to 2001, seismic activity in the Raton Basin was minimal, with only a single M 4 event recorded between 1970 and 2000 (Rubinstein et al., 2014; U.S. Geological Survey Earthquake Hazards Program, 2025). In contrast, between January 2001 and January 2025, the region experienced 19 $M \geq 4$ (U.S. Geological Survey Earthquake Hazards Program, 2025), including a M_W 5.3 event in August 2011 (Barnhart et al., 2014; Rubinstein et al., 2014). Previous studies (Nakai et al., 2017; Glasgow et al., 2021; Wang et al., 2020b; Stokes et al., 2023; Jamalreyhani et al., 2025) have identified that the seismicity is hosted by basement rooted fault segments and studied the spatiotemporal evolution of the seismicity and wastewater injection. However, those studies only estimate M_W for the largest events, and all the other cataloged events only report M_L.

In this study, moment magnitudes are estimated for the Raton Basin from 2016–2024 to examine injection induced seismicity and test small earthquake moment magnitude estimation with a large seismic dataset collected using a local seismic network. There is broad motivation to understand if injection induced earthquake sequences can be distinguished from natural tectonic sequences based on quantitative seismic attributes (Cochran et al., 2024b). In some cases, especially with proximal recording during injection, there is clearly different statistical behavior (e.g. Bachmann et al., 2012; Kwiatek et al., 2019) for events that occur in small areas ($< 5\,\mathrm{km}^2$). In other cases, such as the Raton Basin or the Sichuan Basin (China), earthquake statistics at a local–regional scale appear similar to those in natural tectonic settings (Glasgow et al., 2021; Wang et al., 2020b; Lei et al., 2017; Jamalreyhani et al., 2025). The study area provides an extensive earthquake catalog with ~90,000 events observed between 2016–2024, among which the $M_W \approx 2.5$–4 events are reported with waveform-inversion based moment magnitudes. Using earthquakes in the Raton Basin from 2016–2024, we determine M_W for tens of thousands of events and compare them to M_L while estimating how these differences influence b-values in the Gutenberg–Richter relationship. This analysis aims to address three key questions: (1) How do M_W estimates compare to local magnitude M_L estimates as magnitude decreases? (2) Is there a simple scaling relationship between M_L and M_W? (3) How do b-value estimates in the Gutenberg–Richter law change when using M_L versus M_W?

2 Data and Methodology

2.1 Earthquake catalog and instrumentation

We use earthquake data from events reported in an updated catalog (Jamalreyhani et al., 2025) of the Raton Basin. A previous study (Glasgow et al., 2021) developed an earthquake catalog for the same region, but it contains fewer events because it analyzed a shorter time period. Therefore, we only use events reported in Jamalreyhani et al. (2025). This catalog contains 95,993 events between August 2016 and July 2024. The events were detected using all eight of the publicly available broadband stations in the Raton Basin, which provides about 30 km inter-station spacing. The broadband stations have a sampling rate of 100 Hz. Seismic phases were obtained using a machine-learning phase picker

(PhaseNet; Zhu and Beroza, 2018), trained with manual picks from northern California to detect P- and S-wave arrivals. Previously, Glasgow et al. (2021) showed that PhaseNet performs well in the Raton Basin, detecting phase picks within one tenth of a second in comparison with 50,000 manual picks.

The earthquake locations were obtained using hypoDD (Waldhauser and Ellsworth, 2000) for relocated events or the Rapid Earthquake Association and Location method (REAL; Zhang et al., 2019) when they could not be relocated. The events are located at depths between 0 and 14 km, and their magnitudes range from -1 to 4.2. The local magnitudes reported by Jamalreyhani et al. (2025) were estimated in a similar fashion to the classic method proposed by Gutenberg and Richter (1956). The local magnitudes were estimated using the equation from Glasgow et al. (2021):

$$M_L = \log_{10}(A) + 2.56\log_{10}(D) - 4.6 \tag{1}$$

where A represents the maximum three-component vector amplitude (in micrometers), and D is the distance (in km). The 3-component waveforms were filtered from 0.01 to 40 Hz, corrected for instrument response, and converted to Wood-Anderson displacement. Moment magnitudes for 90 events are available from full Moment Tensor (MT) inversions, where 27 are reported by Glasgow et al. (2021) and an additional 73 were constrained by Jamalreyhani et al. (2025). The MT inversions were performed using either the Time Domain Seismic Moment Tensor package (Dreger, 2003) or a probabilistic waveform inversion implemented in the open-source software package Grond (Heimann et al., 2018). Both methods provide similar values of M_W for the same event with average differences of 0.08. We refer to the set of events with moment magnitudes from MT inversions as "M_W^{MT}". Figure 1 shows a map of the earthquakes and the seismic stations in the Raton Basin.

2.2 Earthquake moment magnitudes from envelope inversion

The Qopen method (Eulenfeld and Wegler, 2016; Eulenfeld et al., 2021) for coda envelope analysis was used to calculate attenuation parameters (scattering and intrinsic), site amplification terms, and source displacement spectra. Our objective is to obtain moment magnitudes, and therefore we focus on the latter result of the source displacement spectra. We chose the Qopen method over others because coda-based approaches are less sensitive to radiation pattern effects, its open access software has been tested in recent publications (Eulenfeld et al., 2023; Eken, 2019; Eulenfeld and Wegler, 2017), and it is well-suited to a small network of stations like we have for the Raton Basin. Additionally, the Qopen method is based on a physical model and does not require calibration or information from previous events. The method has been applied to investigate source parameters at multiple regions with different network geometries including the community stress drop validation study of the 2019 Ridgecrest earthquake sequence (Baltay et al., 2024), earthquakes recorded by a local network in an enhanced geothermal system in Helsinki (Eulenfeld et al., 2023), earthquakes in the Anatolian Fault Zone (Turkey) (Eken, 2019; Izgi et al., 2020), and an earthquake swarm near the Czech–German border region. An earlier version of the method was used to investigate regional earthquakes in Germany (Sens-Schönfelder and Wegler, 2006).

A complete description of the method can be found in Eulenfeld et al. (2021) and Eulenfeld and Wegler (2016). Here, we describe the key steps of Qopen.

The method is based on the radiative transfer theory and uses Paasschen's equation (Paasschens, 1997) to calculate the Green's functions. The synthetic *S*-wave energy density envelopes (E_{syn}) in a given frequency band can be described with the equation:

$$E_{syn}(t,r) = WRG(t,r,g)e^{-bt} \tag{2}$$

where W is the spectral source energy of the earthquake, R is the site amplification factor at each station, and e^{-bt} describes the exponential intrinsic damping that depends on the absorption parameter b. The Green's function $(G(t,r,g))$ with scattering strength g accounts for the direct wave and the scattered wave field and is given by the approximation of the solution for 3D isotropic radiative transfer of Paasschens (1997). The synthetic envelopes are compared with the observed envelopes (from the three-component filtered velocity seismograms, $\dot{u}_c$), given by:

$$E_{obs}(t,r) = \frac{\rho\Sigma_{c=1}^{3}(\dot{u}_c(t,r)^2 + H(\dot{u}_c(t,r))^2)}{2C\Delta f} \tag{3}$$

where H represents the Hilbert transform, ρ is the mean mass density, C represents the energy-free surface correction (equal to 4), Δf is a specific frequency bandwidth. We choose the following central frequencies of the band-pass filters for the broadband array: 0.75, 1.06, 1.5, 2.1, 3.0, 4.2, 6.0, 8.5, 12.0, 17.0, 24.0, and 35.0 Hz. The lower central frequency limit was chosen based on the theoretical corner frequency of the largest magnitude event ($M = 4.2$) in our catalog which corresponds to corner frequencies $\geq$ 1Hz. The upper central frequency limit (35 Hz) was chosen based on the largest frequency when taking into account the width from the central frequency (46.6 Hz) and the Nyquist frequency (50 Hz) of the seismic instrument. Because the inversion is performed in different frequency bands, the parameters W, R, g, and b are determined as functions of frequency f. The spectral source energy $W(f)$ is converted to the *S*-wave source displacement spectrum $\omega M(f)$ with:

$$\omega M(f) = \sqrt{\frac{5\rho v_s^5 W(f)}{2\pi f^2}} \tag{4}$$

where W indicates the radiated *S*-wave energy at a central frequency f, while v_s and ρ represent the mean *S*-wave speed and medium density, respectively. We adopted $\rho = 2,600$ kg/m^3 and $v_s = 3086$ km/s, as used in Glasgow et al. (2021) and Wang et al. (2020b). We selected these values because they match those in the 1D

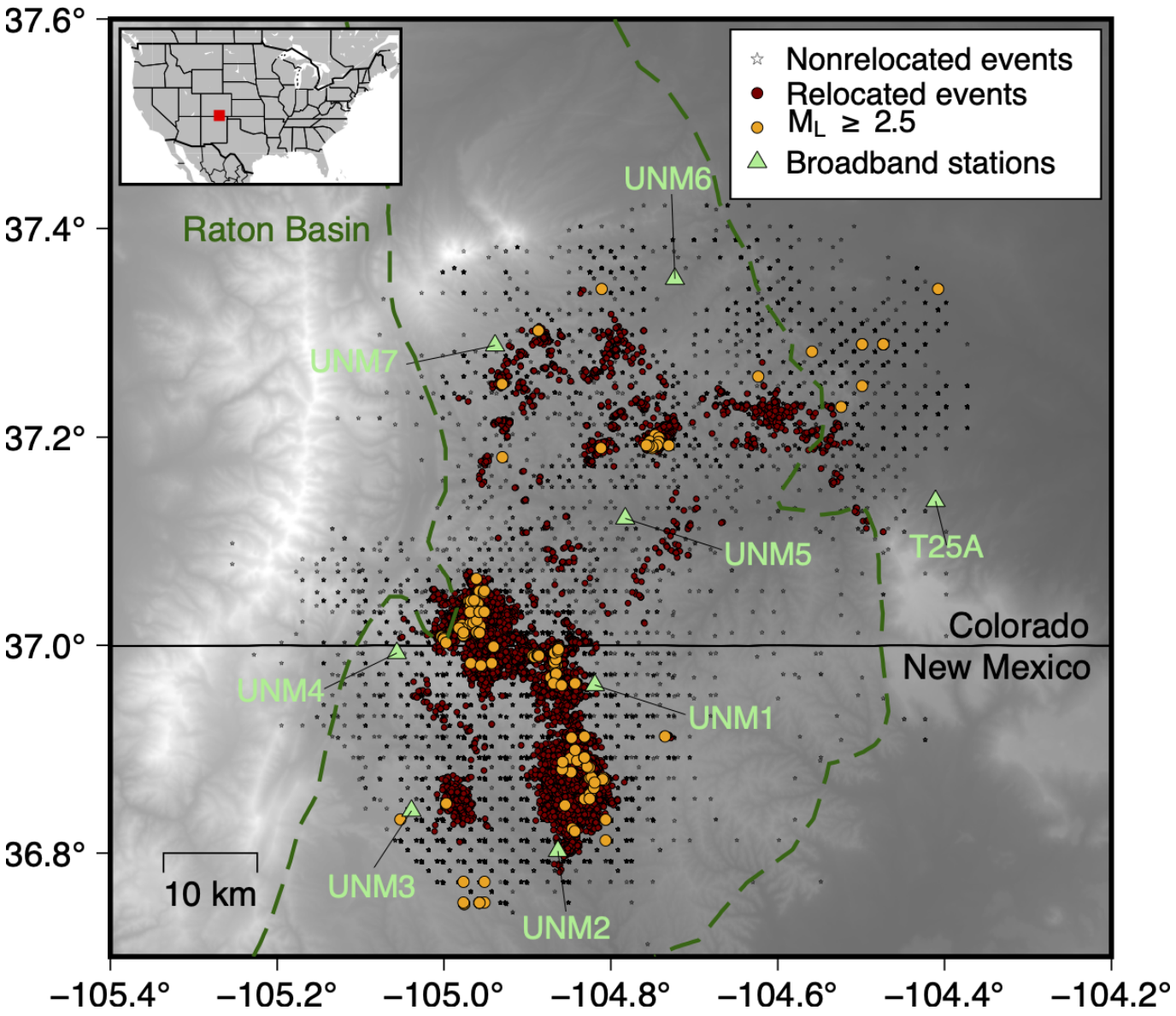

Figure 1 Map of earthquakes and seismic stations in the Raton Basin region that extends across southern Colorado and northern New Mexico, USA. Broadband seismic stations are shown as light green triangles with their respective names. Earthquakes from the catalog of Jamalreyhani et al. (2025) are plotted with red circles showing relocated earthquakes using hypoDD (Waldhauser and Ellsworth, 2000) and stars showing events with locations using REAL (Zhang et al., 2019). Yellow circles represent events with $M_L \geq 2.5$. The Raton Basin is highlighted with the dashed dark green contour. Inset on the top left shows the United States, with the red rectangle indicating the study region.

velocity model at the depths where most events are located. Then the source displacement spectrum is fitted by a source model of the form:

$$\omega M(f) = M_0 \left(1 + \left(\frac{f}{f_c}\right)^{\gamma n}\right)^{-\frac{1}{\gamma}} \quad (5)$$

with seismic moment M_0 and corner frequency f_c (Abercrombie, 1995). n is the high-frequency fall off, and γ is the shape parameter. For simplicity, we fix γ to 2 and keep f_c, n, and M_0 as free parameters.

In this study, we used a direct S-wave window starting 0.25 s before the S- arrival with a length of 4.5 s. The coda window starts at the end of the corresponding direct wave window and ends 100 s after the S-wave onset or earlier if the envelope falls under a signal-to-noise ratio of 2. Additionally, the coda is cut at the smallest possible local minimum if the envelope at a subsequent local maximum is larger by a factor of 3. This criterion effectively removes any possible interfering aftershocks or other large noise signals. We remove a station's data from the inversion if its coda window is shorter than 8 s (i.e., due to the signal-to-noise ratio dropping to 2 too quickly). We discard a specific frequency band for an event entirely if fewer than two stations remain after the previous step. Data in the direct S-wave window are averaged. Furthermore, observed and modeled envelopes are smoothed with a 2-s long central moving average. The equation

$$\ln E_{obs}(t,r) = \ln E_{syn}(t,r) \quad (6)$$

is solved in a least-squares manner.

The inversion can be summarized in the following three steps: (i) Estimate intrinsic and scattering attenu-

ation. The parameters b, g, R, and W are inverted individually for each frequency band and earthquake using the least-squares linear equation system. Because b and g are properties of the medium, both values are fixed for the following steps. Moreover, b and g can be converted to Q-values (see Supplemental Figure S1). At this step, we use only the events with $M_L \geq 2.5$ (shown as yellow circles in Figure 1) to guarantee that the coda is long enough to help separate the two attenuation mechanisms. (ii) Refine and align station site amplification. Equation 6 is solved again only for R and W for each frequency band and earthquake individually. To fix the colinearity between W and R, the site amplification factor of a single station or the geometric mean of site amplification of all stations is fixed to 1. In our case, we fixed the geometric mean to 1. The R-values are geometrically averaged in each frequency band for each station for the final step. We obtain site amplification for each station and frequency band (see Supplemental Figure S2). (iii) Calculate source displacement spectra, source parameters, and moment magnitudes. Equation 6 is again solved for values W using the fixed values g, b, and R determined in previous steps. At this step, we used all events in the catalog. The spectral source densities are converted to displacement (Equation 5) and moment magnitudes can be determined with Equation 5. Figure 2 shows observed and synthetic envelopes for a single earthquake with a $M_L = 3.5$ in the 4–8 Hz frequency band and Supplemental Figure S3 shows the source displacement fit obtained with Equation 5.

2.3 Gutenberg–Richter Law, Magnitude of Completeness and *b*-values

The Gutenberg–Richter law states that earthquake magnitudes are exponentially distributed as

$$\log_{10}(N) = a - bM, \tag{7}$$

where N is the number of earthquakes with magnitudes greater or equal to M. a describes the total number of earthquakes, while the parameter b (also called b-value) measures the relative number of large earthquakes compared to small earthquakes. The b-value is generally about 1 at a global scale or for its two hemispheres (El-Isa and Eaton, 2014). At the laboratory, local, or regional scales, several studies (e.g., Kwiatek et al., 2014; Goebel et al., 2013; Benz et al., 2015; Thapa et al., 2025; Matsumoto et al., 2024) have shown that the b-value exhibits significant spatial or temporal variations. Such variations might be attributed to interactions between fault structures and pore-pressure (Shelly et al., 2016), differential stresses (Goebel et al., 2013), faulting style (Schorlemmer et al., 2005), or pressure and temperature conditions (Wiens, 2001).

Estimating the magnitude of completeness (M_C) is a foundational step for calculating the b-values. The M_C of an earthquake catalog is the lowest magnitude for which all earthquakes in a region are reliably detected by a seismic network. The b-value is sensitive to M_C, an underestimation of M_C may artificially lower the b-value, while an overestimation of M_C reduces the usable data range and increases uncertainty.

Multiple methods have been proposed to obtain M_C. We use the following approaches to determine M_C: (i) the Maximum Curvature (MaxC) technique (Wiemer and Wyss, 2000), (ii) the Goodness of Fit Test (GFT; Wiemer and Wyss, 2000), (iii) M_C by b-value stability (MBS; Cao and Gao, 2002) and (iv) M_C by Coefficient of Variation (MCV) techniques (Godano et al., 2024b) that can be considered a generalization of Cao and Gao (2002). For the M_C obtained with the MaxC technique, we include a correction of $+0.2$ as suggested by Woessner and Wiemer (2005). Additionally, we define the acceptable M_C range as the minimum and maximum values from these methods. Given that the choice of M_C directly impacts the b-value, we focus on the M_C obtained by Godano et al. (2024b) method since the other methods might generate overestimations or underestimations of the M_C (Woessner and Wiemer, 2005), although we confirm that our conclusions hold across all methods.

Once we compute the M_C and its acceptable range using the methods previously mentioned, then we proceed to estimate the b-value. We used multiple methods to estimate the b-value: (i) the maximum-likelihood estimation (MLE) method (Aki, 1965; Bender, 1983), which states that:

$$b_{MLE} = \frac{\log_{10}(e)}{(\bar{M} - M_C + \delta)} \tag{8}$$

where $\bar{M}$ is the average magnitude of events, M_C is the minimum (completeness) magnitude, and δ is one half of the magnitude bin size (e.g. 0.05), which corresponds to a correction for finite bin width (Utsu, 1966). Shi and Bolt (1982) suggested the following formula for the standard deviation of b_{MLE}:

$$\sigma_b = \ln(10) b_{MLE}^2 \sqrt{\frac{\sum_{i=1}^{N}(M_i - \bar{M})^2}{N(N-1)}} \tag{9}$$

where M_i is the magnitude for event i above M_C.

(ii) The b-positive (b_+) method (van der Elst, 2021) uses the positive magnitude difference between successive events, and the b-value is obtained by:

$$b_+ = \frac{\log_{10}(e)}{(\overline{|M'|} - M'_c)} \tag{10}$$

where $\overline{|M'|}$ is the mean of the positive and successive magnitude differences where $M' \geq M'_c$ and M'_c is a minimum magnitude difference threshold not lower than the bin size. We use a $M'_c = 0.2$ as suggested by van der Elst (2021), but we show that other M'_c values lead to similar results.

(iii) the b-more-positive (b_{++}) method (Lippiello and Petrillo, 2024) is an extension of the b_+ method that includes all possible magnitude differences (not only successive ones) and is defined as:

$$b_{++} = \frac{\log_{10}(e)}{(\overline{|M'|}_l - M_{th})} \tag{11}$$

where $\overline{|M'|}_l$ denotes the average magnitude difference for all $\Delta M = m_{i+l} - m_i$, where $l \geq 1$. M_{th} is a threshold value. We show that different M_{th} values lead to similar

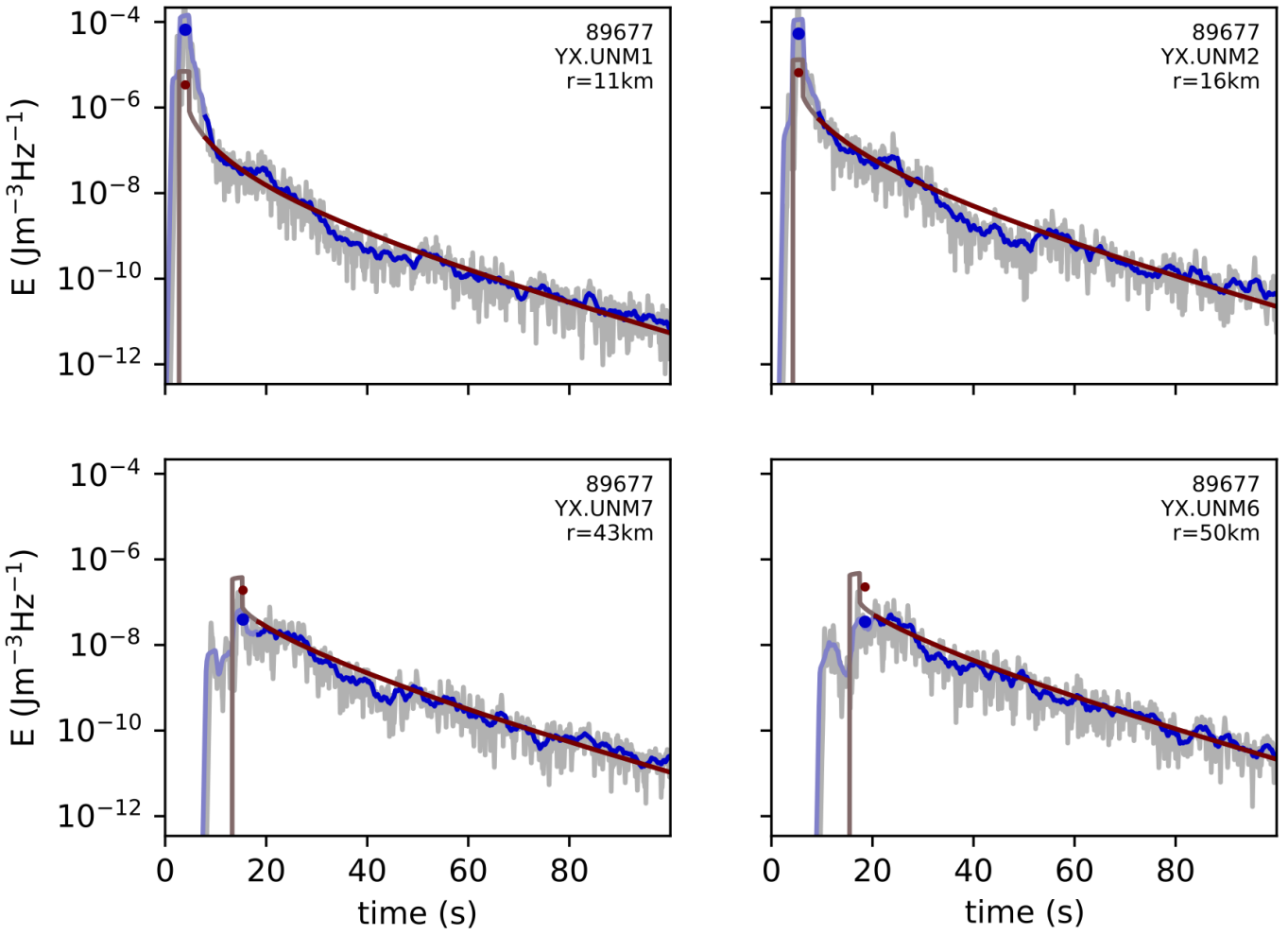

Figure 2 Fits between observed and modeled energy densities for the inversion of an M_L 3.47 event in the frequency band 4–8 Hz. Displayed in each panel are the observed envelope (gray), smoothed observed envelope (blue), and smoothed synthetic envelope (red). The mean of the observed and modeled envelopes in the *S*-wave window are indicated with blue and red dots, respectively. Event ID (89677), network, station name, and distance to hypocenter are indicated in each panel.

conclusions. We use a value of $l = 10$, as suggested by Lippiello and Petrillo (2024).

(iv) The K–M slope (KMS) method (Li and Luo, 2024; Li et al., 2023) can be defined as the slope of the curve between event magnitudes (M) and connectivity degrees (K, a parameter from topological analysis) in a seismic sequence. As shown by Li et al. (2023), the K–M slope obtained from visibility graph analysis is proportional to the b-value. (v) A simple least-squares fit (LF) regression to the magnitude–frequency distribution (El-Isa, 2013; El-Isa and Eaton, 2014).

3 Results

3.1 Moment Magnitudes and relationships with other magnitude types

From the original catalog of 95,993 events, we successfully obtained M_W values for 31,581 events using the Qopen method applied to broadband seismic data. This subset of common events ($n = 31,581$) is referred to as M_W^{Qopen} when M_W is derived from Qopen and as M_L^{SJ25} when referring to M_L values reported in Jamalreyhani et al. (2025). The magnitude range for M_W^{Qopen} is 0.42 to 4.43, while for M_L^{SJ25} it is -1 to 4.25. We were unable to determine M_W for a large fraction of the catalog ($\approx 2/3$) because the coda envelopes had low SNR (< 2) or short coda durations (< 8 s). Figure 3a presents a comparison between M_W^{Qopen} and M_L^{SJ25}. We observe good agreement between M_W^{Qopen} and M_L^{SJ25} for events with $M > 3$, but note a systematic difference between the two scales for events smaller than $M_L < 3$.

We also compare the events with M_W^{Qopen} in the Raton Basin reported in the Advanced National Seismic System Comprehensive Catalog (ComCat; U.S. Geological Survey Earthquake Hazards Program, 2025). There are 1,124 common events between the M_W^{Qopen} and ComCat events of any magnitude type. The ComCat preferred magnitude type can differ by event; here, we find matching events of the following type: 1,069 with local magnitude (M_L^{CC}), 37 with short-period Lg waves (M_{bLg}^{CC}), and 20 with moment magnitudes (M_{wr}^{CC}). We use the superscript ^{CC} to refer to the events in ComCat. Moment magnitudes from MT inversions are less commonly reported and are usually only available for relatively large events. Table 1 provides a complete overview of the magnitudes included in our study.

Variable name	Description	Number of events	Magnitude Range
M_W^{Qopen}	Moment magnitudes obtained using envelope inversions in this study.	31,581	0.42–4.43
M_W^{MT}	Moment magnitudes using moment tensor inversions reported by Jamalreyhani et al. (2025); Glasgow et al. (2021)	94	2.32–4.22
M_L^{SJ25}	Subset of events with local magnitudes reported by Jamalreyhani et al. (2025) that also have a moment magnitude from M_W^{Qopen}.	31,581	-1.04–4.25
M_{wr}^{CC}	Moment magnitudes derived from moment tensor inversion of the whole seismogram at regional distances reported in Comcat (U.S. Geological Survey Earthquake Hazards Program, 2025).	20	3.2–4.3
M_L^{CC}	The original magnitude relationship defined by Gutenberg and Richter in 1935 for local earthquakes reported in Comcat (U.S. Geological Survey Earthquake Hazards Program, 2025).	1,069	0.3–4.8
M_{bLg}^{CC}	Magnitude for regional earthquakes based on the amplitude of the Lg surface waves as recorded on short-period instruments reported in Comcat (U.S. Geological Survey Earthquake Hazards Program, 2025)	38	1.4–3.4

Table 1 Summary of magnitude scales used in this study, including their descriptions, number of events, and magnitude ranges.

Comparisons between M_W^{Qopen} and ComCat magnitudes (Figure 3b–c) reveal trends similar to those observed with M_L^{SJ25}: good agreement for events around $M \approx 3$ but increasing divergence for smaller events ($M < 2.5$). The other ComCat magnitudes (M_{wr}^{CC} and M_{bLg}^{CC}) and M_W^{MT} also align well with M_W^{Qopen}, closely following the 1:1 line.

We examine more closely these differences and agreements between M_W^{Qopen} and all the other magnitude types. Figure 3d shows the distributions of differences (ΔM) between the M_W^{Qopen} and all other magnitudes with box-plots. The median values and interquartile range (IQR) varied across magnitude differences, with the highest value observed for $M_W^{Qopen} - M_L^{SJ25}$ (median $= 0.82$, IQR $= 0.40$), followed by $M_W^{Qopen} - M_L^{CC}$ (median $= 0.62$, IQR $= 0.28$), $M_W^{Qopen} - M_{bLg}^{CC}$ (median $= 0.34$, IQR $= 0.19$), $M_W^{Qopen} - M_w r^{CC}$ (median $= 0.15$, IQR $= 0.18$), and M_W^{MT} (median $= 0.1$, IQR $= 0.12$), reflecting systematic scaling differences between the local magnitude scales and M_W^{Qopen}. The IQRs were narrower for $M_W^{Qopen} - M_W^{MT}$ and $M_W^{Qopen} - M_{wr}^{CC}$, indicating consistency between different moment magnitude estimations.

The large differences between M_W and M_L presented here have been observed in other regions (Ross et al., 2016; Moratto et al., 2017) and are theoretically expected as a consequence of a combination of factors (Deichmann, 2006, 2017): anelastic attenuation, which removes much of the high-frequency energy of small earthquakes, and the instrument response of the Wood-Anderson typically used to estimate local magnitudes. Notably, even when comparing M_W estimates derived from different methodologies, small but consistent offsets, similar to what we report ($\Delta M \approx 0.15$), persist. For example, Shelly et al. (2021) suggested that differences of 0.1–0.2 are common between different (waveform-modeled) M_W estimates, and Holt et al. (2021) reported similar differences ($\sim$ 0.2) between M_W from coda methods, moment tensor inversions, and direct spectral modeling methods for events in Utah (see Figure 11c in Holt et al., 2021).

We used Orthogonal Distance Regressions (ODR) to quantify the relationships between M_W^{Qopen} and other magnitudes (dashed lines in Figures 3a–c). We favor ODRs over least-squares linear regressions because the latter can introduce systematic errors in magnitude conversion equations (Castellaro et al., 2006; Castellaro and Bormann, 2007). First, we examine the relationships between M_W^{Qopen} and M_L^{SJ25} and between M_W^{Qopen} and M_L^{CC}. The relationships we determined are $M_W^{Qopen} = 0.70 M_L^{SJ25} + 0.96$ (gray dashed line in Figure 3a) and $M_W^{Qopen} = 0.73 M_L^{CC} + 0.99$ (gray dashed line in Figure 3b), respectively. These relationships suggest that local magnitude calculations underestimate the true size of earthquakes in the Raton Basin. The underestimation is clear for small magnitude events; for example, a $M_L = 1$ reported in ComCat could correspond to a $M_W = 1.7$, as the event (local) magnitude increases the differences between M_W, and M_L decreases as they approach $M \approx 3$. Our equation is most likely valid for only events with $M_L \leq 3$ and may not apply for events with $M > 3.5$ as the difference between M_W and M_L (0.2; Figure 3a) corresponds to typical uncertainties observed in magnitude estimations. We do not estimate an ODR for the relationship between M_W^{Qopen} and M_{bLg}^{CC} since we have a small population of events ($n < 40$). We also use ODR to quantify the relationship of M_W^{Qopen}, M_{wr}^{CC} and M_W^{MT}. Figure 3c (red dashed line) shows the M_W data and the relationship obtained: $M_W^{Qopen} = M_W + 0.09$, which indicates the good agreement among the moment magnitude estimates.

3.2 Magnitude of completeness and *b*-values

We estimate the M_C (magnitude of completeness) and b-values for the common events with M_W^{Qopen} and M_L^{SJ25}. Figure 4 shows the magnitude–frequency distribution of earthquakes for M_L^{SJ25}(Figure 4a) and M_W^{Qopen} (Figure 4b). Table 2 shows the M_C results for all the methods, which ranges between 1.2–1.4 for M_W^{Qopen} and 0.5–0.7 for M_L^{SJ25}. The M_C values obtained using the

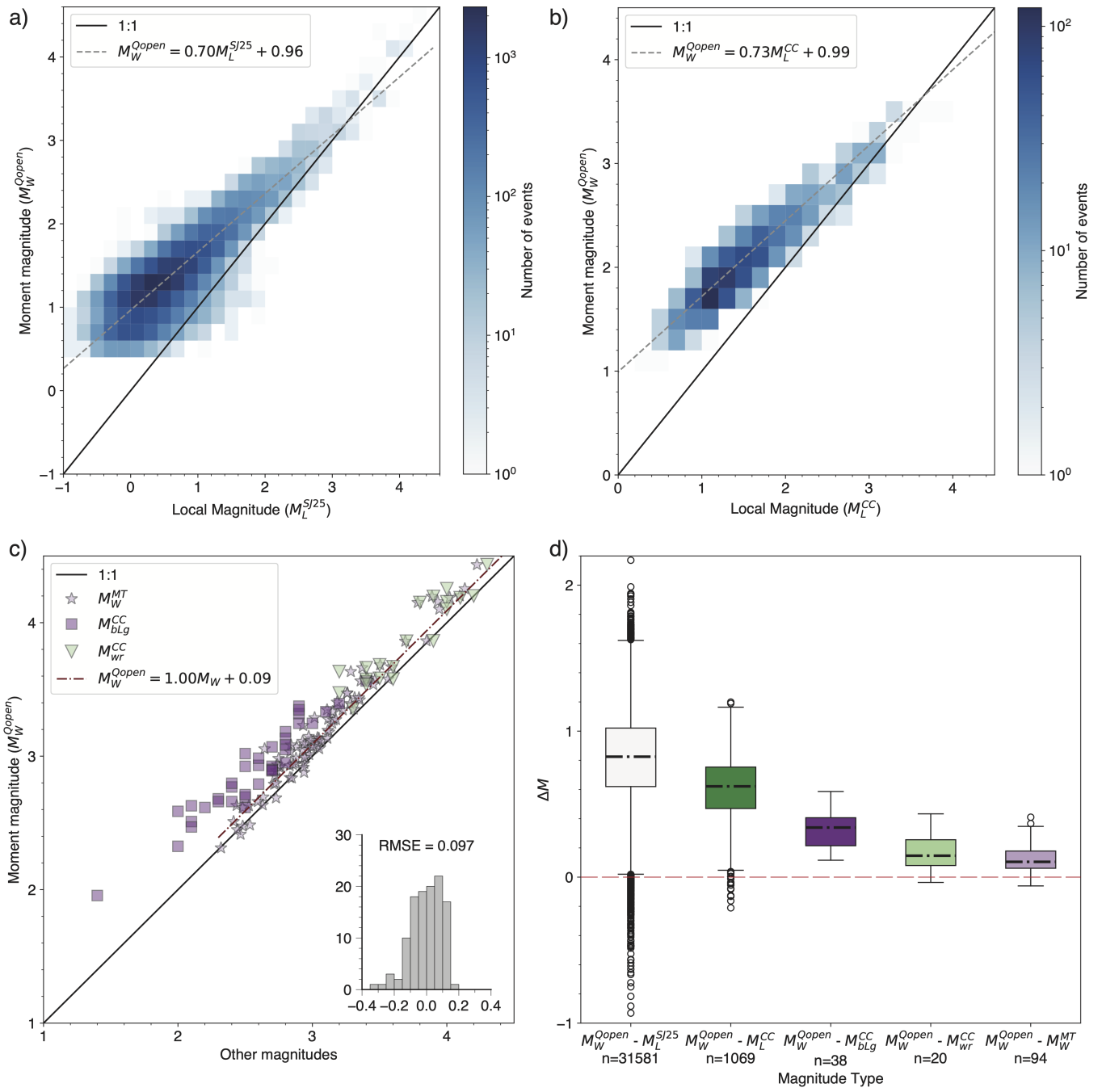

Figure 3 (a) Local magnitudes (M_L^{SJ25}) reported in Jamalreyhani et al. (2025) versus moment magnitudes (M_W^{Qopen}) obtained in this study. (b) Local magnitudes (M_L^{CC}) reported in ComCat (U.S. Geological Survey Earthquake Hazards Program, 2025) versus moment magnitudes (M_W^{Qopen}). Solid lines in (a) and (b) represent a 1:1 relationship. Gray lines represent orthogonal distance regression fits of $M_W^{Qopen} = 0.7M_L^{SJ25} + 0.96$ in (a) and $M_W^{Qopen} = 0.73M_L^{CC} + 0.99$ in (b). (c) Magnitude comparison between moment magnitude estimates from M_W^{Qopen}(y-axis) and other reported magnitudes (x-axis): M_W^{MT} (light purple stars), M_{bLg}^{CC} (purple squares), M_{wr}^{CC} (light green triangles). The solid black line represents a 1:1 relationship while the dashed red line represents an orthogonal distance regression between M_W^{Qopen} and other M_W from moment tensor inversions. The inset at the bottom right is a histogram of the residuals for the regression with the root mean square error (RMSE). The RMSE and overall bias (offset) of 0.09 is below 0.1–0.2, which are typical errors reported for an earthquake magnitude. (d) Box-plots representing the distributions of the magnitude differences (ΔM) between Qopen M_W and each of the other reported magnitudes. The black dashed line on each box-plot represent the median value of each distribution. n represent the number of events. The coloured boxes are limited by the first (Q1) and third quartile (Q3). The upper and lower whiskers represent Q3 $+1.5$ the interquartile range (IQR) and Q1 -1.5IQR, respectively. The points that do not fall within the box-plot or the whiskers are shown as white circles. Horizontal dashed red line shows $\Delta M = 0$.

Godano et al. (2024b) method are 0.5 for M_L^{SJ25} and 1.2 for M_W^{Qopen}. Figure 4a shows that the b-values obtained for M_L^{SJ25} are approximately 1 (0.96–1.03), regardless of the chosen method used to estimate such values. On the other hand, the b-values obtained using M_W^{Qopen} range between 1.25 and 1.37, depending on the method (Figure 4b).

We also examine the stability of the b-value estimate with M_C. Figure 5 illustrates the b-values as a function of M_C for M_L^{SJ25} and M_W^{Qopen}. The acceptable M_C range is 0.5 to 0.7 for M_L^{SJ25} (Figure 5a) and 1.2 to 1.4 for M_W^{Qopen} (Figure 5b). The b-values determined using the different methods across the range of acceptable M_C are similar to those reported above with b-values ≈ 1 for M_L^{SJ25} and b-values ranging between 1.2 and 1.4 for M_W^{Qopen}.

The b-positive (van der Elst, 2021) and b-more-positive (Lippiello and Petrillo, 2024) methods are more robust in comparison with the other methods we applied in our study. However, the minimum magnitude difference (M_C') parameter or the minimum threshold parameters (M_{th}) and how it affects the b-value estimation has been investigated less. Figure 5c and 5d shows the dependency of b_+ versus M_C' and b_{++} versus M_{th} using M_L^{SJ25} and M_W^{Qopen}, respectively, which shows that there is some minor variability on the b-value depending on those two parameters. For example, applying the b-positive method to M_L^{SJ25} with a $M_C' = 0.2$ leads to $b = 0.96$, while using a $M_C' = 0.5$ results in $b = 1.03$. Nevertheless, we note that b_+ and b_{++} values are generally close to 1 when we apply it to M_L^{SJ25}, while b_+ and b_{++} values are overall larger than 1.1 for M_W^{Qopen}.

4 Discussion

4.1 Differences between M_W and other magnitudes for other regions

Theoretical and simulation-based studies (Deichmann, 2017, 2006; Edwards et al., 2010) show that the breakdown between M_W and M_L can be explained as an interaction between the earthquake source, wave propagation or attenuation effects, and the instrument response, in particular the common conversion to a Wood Anderson response as needed to compute M_L. Several previous studies in different regions (e.g., Bakun, 1984; Bethmann et al., 2011; Ben-Zion and Zhu, 2002; Ross et al., 2016; Eken, 2019; Bindi et al., 2020; Malagnini and Munafò, 2018; Moratto et al., 2017; Jost et al., 1998; Archuleta et al., 1982) have observed deviations between M_W and M_L. A few examples include: (i) Munafò et al. (2016) analyzed a high-quality data set of 1,191 small earthquakes in Italy, using random vibration theory, and found that $M_W = \frac{2}{3}M_L + 1.15$ for events in the $0 \leq M_L \leq 3.8$ range, (ii) Bethmann et al. (2011) studied 195 events in Basel (Switzerland), applying spectral fits (Abercrombie, 1995), and determined that $M_W = 0.63M_L + 0.76$ for events in the range of $0.7 < M_L < 3.4$, and (iii) Patton et al. (2025) investigated 85 earthquakes in Nevada using the Coda Calibration Tool (CCT; Mayeda and Walter (1996); Mayeda et al. (2003); Barno (2017)) and established that $M_W = 0.81M_L + 0.47$ for events with $0 \leq M_L \leq 3.0$. For other relationships between moment magnitudes and local magnitudes identified in various regions, we recommend the following studies to interested readers: Dost et al. (2018); Dahm et al. (2024); Deichmann (2006); Hanks and Boore (1984). We highlight that the studies described above estimated M_W using different methods: spectral modeling of direct P- or *S*-waves (Scherbaum, 1990; Abercrombie, 1995; Edwards et al., 2010), moment tensor inversions in the time or frequency domains (Ichinose et al., 2003; Heimann et al., 2018), or coda envelope inversions (Mayeda et al., 2003; Mayeda and Walter, 1996; Eulenfeld et al., 2021), but all concluded that $M_L \neq M_W$ for events $M < 4.0$.

The M_W obtained ranges between 0.42 and 4.43. We show that for low magnitudes ($M_W < 2.5$) there could be a $\sim$ 1 unit magnitude difference between M_W^{Qopen} and the M_L^{SJ25} or between M_W^{Qopen} and M_L^{CC}. We find that $M_W^{Qopen} = 0.70M_L^{SJ25} + 0.96$ and $M_W^{Qopen} = 0.73M_L^{CC} + 0.99$. The slopes we obtain are nearly identical to what has been shown is theoretically expected for small earthquakes(Hanks and Boore, 1984; Deichmann, 2006), which should scale as $\log M_0 \sim M_L$ which translates to $M_W \sim (2/3)M_L$.

These linear relationships suggest that M_L may significantly underestimate the true size of small earthquakes in the Raton Basin, assuming M_W is a more reliable measure of earthquake size. For example: an earthquake with an estimated M_L1.0, using Equation 1, might be as large as a M_W1.66. While these relationships provide a basis for converting M_L to M_W in future studies of the Raton Basin, their application requires caution: for events with $M_L \leq 1.5$, the mean absolute error (MAE $= 0.23$) and root mean square error (RMSE $= 0.18$) indicate that significant magnitude uncertainty is expected when converting M_L to M_W.

We also compare our M_W^{Qopen} estimates with other M_W estimates from MT inversions (Figure 3c). We obtain a regression of $M_W^{Qopen} = M_W + 0.09$, which indicates a large agreement between both estimates with a RMSE of 0.096. The offset of 0.09 and RMSE below 0.2 are typical errors obtained for earthquake magnitude estimations (Shelly et al., 2021) and suggests that M_W determined with Qopen are reliable. A few recent studies have also compared M_W between different methods: (i) Holt et al. (2021) estimate M_W using the CCT and spectral modeling of direct S_g phases (Pang et al., 2020) for the Magna, Utah, earthquake sequence for 280 events, (ii) Eulenfeld et al. (2021) compute M_W using Qopen, Grond (Heimann et al., 2018), and source displacement spectrum from the direct onset of P- and *S*-waves for the 2018 West Bohemia (Czech-German border) earthquake swarm that contains 150 seismic events, and (iii) Morasca et al. (2022) compare M_W estimates using the spectral amplitude decomposition approach also known as Generalized Inversion Technique (GIT; Castro et al. (1990); Andrews (2013)) and the CCT for 247 events in Italy. All of these studies have shown that there is general agreement (differences smaller than 0.13) on M_W obtained with different methods. Less agreement is found among different methods

Method	M_C for M_W^{Qopen}	M_C for M_L^{SJ25}
Maximum curvature technique (Wiemer and Wyss, 2000) with $+0.2$ correction	1.4	0.6
Goodness of fit test (Wiemer and Wyss, 2000)	1.2	0.5
M_C by b-value stability (Cao and Gao, 2002)	1.3	0.7
M_C by coefficient of variation techniques (Godano et al., 2024b)	1.2	0.5
Acceptable range	1.2–1.4	0.5–0.7

Table 2 Summary of the magnitude of completeness (M_C) obtained with different methods for M_W^{Qopen} and M_L^{SJ25}. The acceptable range is defined as the minimum and maximum values by all the methods.

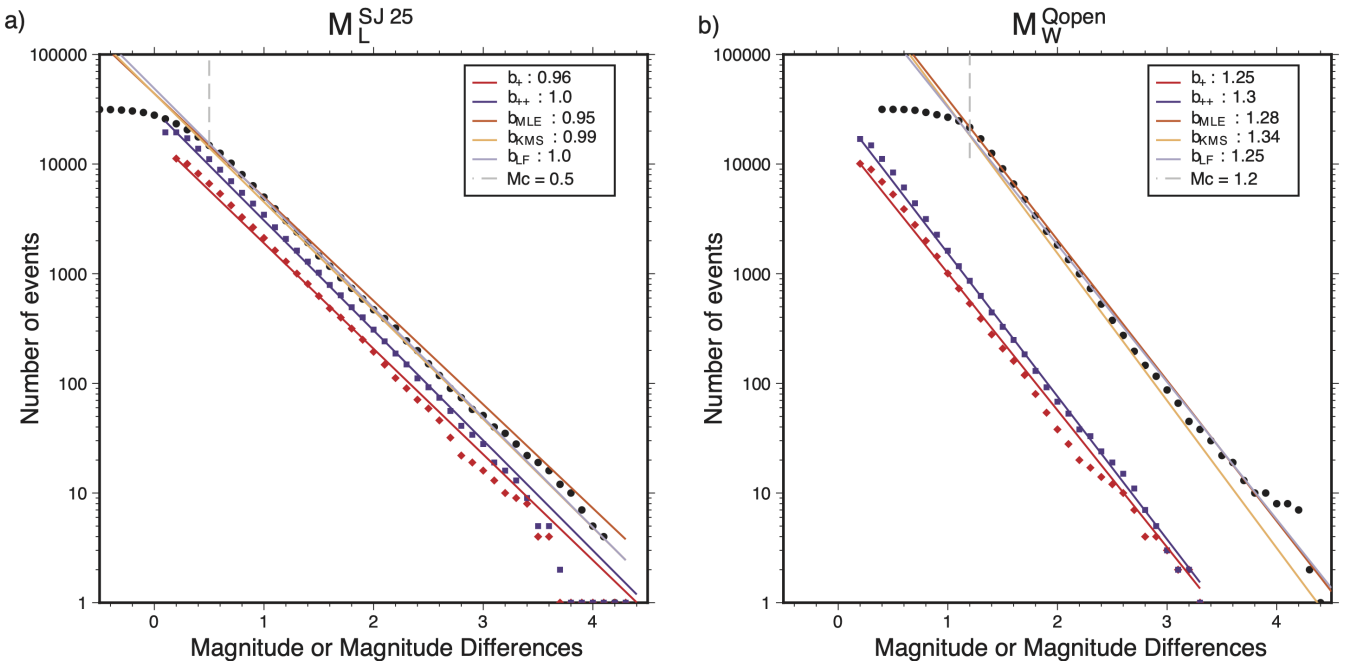

Figure 4 Cumulative magnitude–frequency distribution for (a) M_L^{SJ25} and (b) M_W^{Qopen}. The red diamonds represent the cumulative positive magnitude differences frequency distribution and respective fit with the b-positive method (van der Elst, 2021). The blue squares represent the cumulative magnitude differences frequency distribution and respective fit with the b-more-positive method (Lippiello and Petrillo, 2024). The vertical gray lines represent the magnitude of completeness M_C based on Godano et al. (2024b). Coloured lines represent the b values obtained with different methods: b_+ (b-positive; red line), b_{MLE} (maximum likelihood method; orange), b_{KMS} (K–M slope method; yellow), and b_{LF} (least-squares fit; light purple). The b-values for the events with M_L^{SJ25} range between 0.96–1.03, while the b-values using M_W^{Qopen} ranges between 1.25–1.37.

for the estimation of other source parameters such as corner frequencies (f_c) or stress drops ($\Delta\sigma$) (Cochran et al., 2024a; Baltay et al., 2024). Future research efforts related to source parameters in the Raton Basin might include: (i) use different methods (CCT, GIT, Qopen, etc.) to compare stress drop estimates or (ii) use the available nodal array dataset that includes 95 seismic nodes (code network: 4E) and its respective earthquake catalog (Wang et al., 2020b) to estimate source parameters for even smaller events. We acknowledge that with Qopen (Eulenfeld and Wegler, 2016) we can estimate f_c or $\Delta\sigma$ but for this study we decided to focus only on the size of events (M_W).

4.2 Variations of *b*-values across different regions

In the Raton Basin, previous studies (Glasgow et al., 2021; Jamalreyhani et al., 2025) have reported $M_C \approx 0$ and $b \approx 1$, based on larger catalogs with local magnitudes ($n \approx 38{,}000$ and $n \approx 96{,}000$ events, respectively). For our analysis, we used a subset of 31,581 events for which both M_L^{SJ25} and M_W^{Qopen} magnitudes are available. Although this is smaller than the full catalog ($n = 95{,}993$), a comparison of their frequency-magnitude distributions confirms that this subset does not bias our results. As shown in Figure S4, significant incompleteness in the subset occurs only for magnitudes $M \leq 0$, which is well below the M_C for both the subset and the full catalog. Furthermore, the distributions are highly similar above M_C, and the b-values derived from them are equivalent. It is uncommon to have such a large number of events ($n = 31,581$) with M_W available for b-value estimation as we have here; prior studies with moment magnitudes (Shelly et al., 2021; Ross et al., 2016; Baltay and Abercrombie, 2025) have used far fewer events ($n < 10{,}000$). This is a significant advantage as seismic hazard analyses are often limited by catalogs that are either declustered or culled with a high M_C (i.e., $M_C \geq 3$)

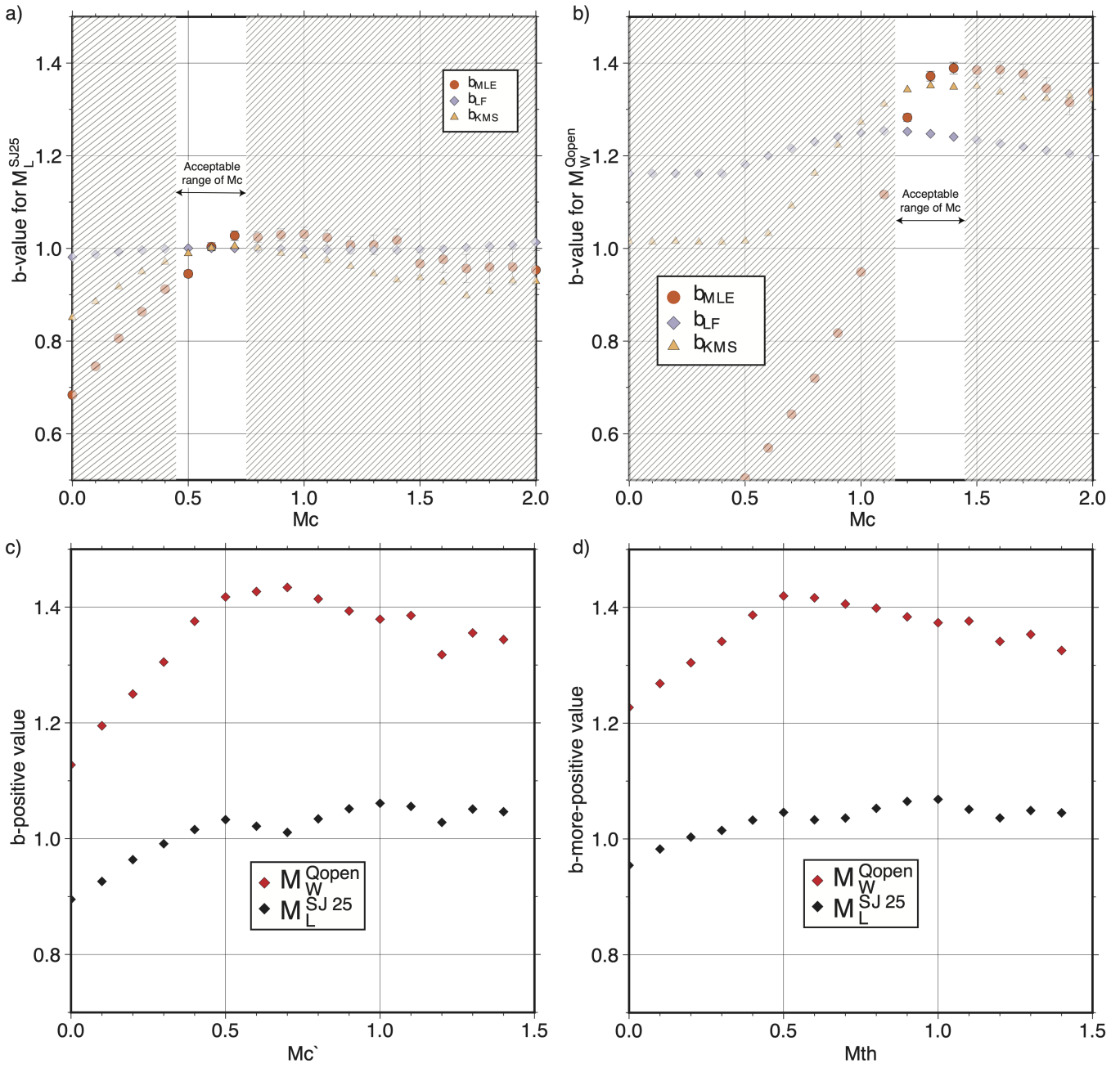

Figure 5 b-values as a function of M_C with (a) M_L^{SJ25} and (b) M_W^{Qopen}. The b-values obtained with the maximum-likelihood estimation (MLE) method (Aki, 1965), least-squares fit (LF) method, and K–M slope (KMS) method (Li and Luo, 2024) are shown as orange circles, light purple diamonds, and yellow triangles, respectively. The acceptable range of M_C represents the range of minimum and maximum values of M_C obtained with different methods: the maximum curvature technique (Wiemer and Wyss, 2000), the goodness of fit test (GFT; Wiemer and Wyss, 2000), and M_C by b-value stability (MBS; Cao and Gao, 2002). The acceptable ranges of M_C are 0.4–0.7 for the M_L^{SJ25} (a) and 1.2–1.4 for the M_W^{Qopen} (b). For the case of M_L^{SJ25}, the b-values range between 0.95–1.02, while for M_W^{Qopen}, the b-values range between 1.25–1.38. (c) b-values using the b-positive method (van der Elst, 2021) as a function of M_C' for M_W^{Qopen} (red diamonds) and M_L^{SJ25} (black diamonds). The b-positive values range between 0.9–1.06 for M_L^{SJ25} and 1.13–1.43 for M_W^{Qopen} depending on which M_C' is chosen. (d) Same as in (c) but using the b-more-positive method (Lippiello and Petrillo, 2024). The b-more-positive values range between 0.95–1.07 for M_L^{SJ25} and 1.23–1.42 for M_W^{Qopen} depending on which M_{th} is chosen.

(Valensise et al., 2024; Taroni and Akinci, 2020; Teng and Baker, 2019).

Numerous methods exist for estimating M_C (Wiemer and Wyss, 2000; Cao and Gao, 2002; Godano et al., 2024b; Lombardi, 2021; Godano, 2017; Wang et al., 2025; Amorese, 2007; Ogata and Katsura, 1993; Taroni, 2023). In this study, we tested four of these methods (see Table 2) on events with M_L^{SJ25} and M_W^{Qopen}, which yielded M_C ranging between 0.5–0.7 and 1.2–1.4, respectively. This dependence of M_C on the magnitude type is perhaps expected as M_W values are systematically higher than M_L values, naturally leading to a higher M_C when M_W is used. The accuracy of any M_C estimate is inherently dependent on the number of samples and the

shape of the magnitude–frequency distribution. Furthermore, the methods themselves have known biases: the MBS method can overestimate M_C (Lombardi, 2021; Zhou et al., 2018), while the MaxC method tends to underestimate it (Mignan and Woessner, 2012; Zhou et al., 2018; Woessner and Wiemer, 2005), often adding an arbitrary $+0.2$ correction. The GFT method's performance is variable, potentially leading to either underestimation or overestimation depending on the dataset (Woessner and Wiemer, 2005; Zhou et al., 2018). Although the MCV method has been tested on various regions (California, Italy, New Zealand, and Japan) and synthetic catalogs (Godano et al., 2024a,b), its performance in other tectonic settings requires further validation.

Figure 4 shows the b-values obtained with different methods using the M_C from the MCV method, which in turns reveals the dependency of the b-value on the magnitude type. With M_L^{SJ25}, the b-value is consistently near 1.0, while with M_W^{Qopen}, it corresponds to values above 1.2 (Figure 4). This dependency persists even when considering the full range of M_C estimates from other methods: for M_L^{SJ25}, the b-value remains stable around 1.0 (Figure 5a), and for M_W^{Qopen}, it varies between 1.2 and 1.4 (Figure 5b). Ultimately, Figure 5 demonstrates that the b-value is inherently tied to the magnitude scale, regardless of the specific M_C or b method chosen.

We now address some of the limitations of the methods used to estimate b-values. The b_{MLE} method (Aki, 1965) (and its modified formulations) has been widely applied in previous studies of earthquake sequences and high-resolution catalogs (Warren-Smith et al., 2017; Spassiani et al., 2023; Pezzo et al., 2023; Tan et al., 2021). However, the b_{MLE} method may be subject to biases (Marzocchi et al., 2019; Geffers et al., 2022) due to factors such as: (i) large binning sizes (0.2 or higher), (ii) a dynamic range (the difference between the maximum magnitude and M_C) of less than 2 magnitude units, or (iii) a small population of events ($n < 1,000$). In the Raton Basin, the b_{MLE} yields values of 1.03 for M_L^{SJ25} and 1.37 for M_W^{Qopen} (orange lines in Figure 4), indicating a significant increase between magnitude types. This increase cannot be easily attributed to the biases noted above as: (i) we used a binning size of 0.1, (ii) the dynamic range in our dataset exceeds three magnitude units, and (iii) our analysis includes a large population of earthquakes ($n > 10,000$).

The b_{KMS} method (Li et al., 2023), though less commonly used than b_{MLE}, also suggests higher b-values for M_W compared to M_L (1.35 versus 1.0; light orange lines in Figure 4). Similarly, the least-squares regression method (b_{LF}) shows an increase in b-values when switching from M_L^{SJ25} to M_W^{Qopen}, from 1.0 to 1.25. The b_{LF} method is generally discouraged due to its tendency to underestimate b-values (Castellaro et al., 2006; Sandri and Marzocchi, 2007; Geffers et al., 2022), as it weights high-magnitude events (small samples) the same as low magnitude events (large samples). Nevertheless, some studies continue to apply it (El-Isa and Eaton, 2014; Ibáñez et al., 2012). Despite its limitations, our results using b_{LF} are consistent with those obtained from other methods.

Some of the most robust methods for estimating b-values are the b_+ method (van der Elst, 2021) and the b_{++} method (Lippiello and Petrillo, 2024) because they are relatively insensitive to transient changes in completeness, such as short-term aftershock incompleteness or evolving seismic network configurations. We still observe that changing the magnitude scale from M_L^{SJ25} to M_W^{Qopen} results in an increase in the b_+ from 0.96 to 1.25 and for the b_{++} from 1.0 to 1.3. There are several reasons why b-values in earthquake catalogs may be underestimated or overestimated. In this study, we tested multiple methods to estimate b-values for the Raton Basin and found that the results differ depending on whether M_L or M_W magnitudes are used.

The influence of magnitude scale choice on b-values remains surprisingly understudied, despite well-documented discrepancies between M_L and M_W for small earthquakes spanning multiple regions and decades. While a simple offset between scales might not affect b-values, some studies have shown the opposite: (i) Ross et al. (2016) found $b = 1.22$ using M_W versus $b = 0.93$ with M_L for $> 11,000$ events in the San Jacinto Fault Zone (California). (ii) Shelly et al. (2021) obtained $b = 1.18$ (M_W) versus 1.60 (converted M_L to M_W) in northern Oklahoma and $b = 1.06$ (M_W) versus 1.40 (converted M_L to M_W) in Kansas, though both values were limited by small sample sizes ($n < 100$). (iii) Frohlich and Davis (1993) found significant differences between b-values for different teleseismic earthquake catalogs when using different magnitude scales. (iv) Baltay and Abercrombie (2025) did not report b-values but show that the slope of the magnitude frequency distribution is ~ 1 with M_W and $\sim 3/4$ with M_L for a subset of events that belong to the Ridgecrest 2019 earthquake sequence. These findings align with our Raton Basin observations, where b-values changes with the magnitude scale chosen. Therefore, we expect that other seismically active regions might also have different b-values if local magnitudes are used instead of moment magnitudes.

Different b-values (0.5–2.9) have been observed in regions with induced seismicity (Mousavi et al., 2017). For instance: (i) Kwiatek et al. (2015) observed a b-value of 1.2 for a small cluster of earthquakes ($n = 1,275$), with converted magnitudes from magnitude duration to M_W, located in the northwestern part of the Geysers geothermal field (California), (ii) Kozłowska et al. (2018) identified two groups of seismicity induced by hydraulic fracturing in Ohio with b-values of 1.5 and 0.7 with M_L, (iii) Kwiatek et al. (2010) determined a b-value of 1.26 for small mining-induced events in South Africa with M_W, and (iv) McMahon et al. (2017) obtained a b-value of 0.5 with relative magnitudes for the 2011 Prague, Oklahoma earthquake sequence likely induced by deep wastewater injection. Moreover, there will be some variability for b-value obtained by different studies even for the same region for several reasons: using different catalogs, using different magnitude scales, applying different methods for estimating M_C and/or b-value. A clear example of such variability

was shown by Gable and Huang (2024), where they determine b-values using the b_{MLE} (Aki, 1965) and the b_+ method (van der Elst, 2021) for different catalogs of the 2011 Prague, Oklahoma earthquake sequence that contain local magnitudes (Skoumal et al., 2019), moment magnitudes (Cochran et al., 2020a), or relative magnitudes, and found b-values ranging between 0.57–0.99 depending on the method and magnitude used. In the Raton Basin, previous studies (Jamalreyhani et al., 2025; Wang et al., 2020b; Glasgow et al., 2021) have reported b-values close to 1; we obtain similar b-values with M_L^{SJ25} on the range of 0.96–1.03, while we obtain $b = 1.25$–1.37 when using M_W^{Qopen}. Such increase in the b-value may affect any previous probabilistic seismic hazard estimations (Petersen et al., 2018), physics-based forecast seismicity models (Hill et al., 2024), or statistical analysis (Glasgow et al., 2021; Wang et al., 2020b) in the Raton Basin.

4.3 Implications, recommendations, and some limitations

Higher b-values in the Raton Basin may indicate a decrease in the estimated seismic hazard, as they correspond to a lower likelihood of large earthquakes. However, seismic hazard assessment in induced seismicity regions remains complex, as small-magnitude events can still have societal impacts. Some of the small earthquakes are felt by nearby towns, such as Trinidad, Colorado, and Raton, New Mexico. We found that 41 earthquakes were reported as felt[1] with responses ranging from 1 to 15, according to the USGS 'Did You Feel It?' database (Wald et al., 2012), for events with local magnitudes less than or equal to 3.0 during the same time period covered in our analysis (2016–2024). Some studies (Langenbruch and Zoback, 2016; Langenbruch et al., 2018) argue that, in regions of induced seismicity such as Oklahoma, Kansas, and the Raton Basin, physics-based models are preferable to probabilistic seismic hazard analysis (PSHA) (Petersen et al., 2017, 2018). This is because PSHA does not account for injection rates at varying locations and times. Physics-based models inherently depend on b-values and a monthly earthquake rate for events exceeding a specific magnitude. Hill et al. (2024) developed such a model for the Raton Basin, enabling the forecasting of induced seismicity in both space and time across the basin. While it is difficult to assess how b-values might influence such physics-based forecasts, the earthquake rate will vary depending on the selected magnitude threshold (and the magnitude scale used) according to our results. For instance, if we only consider the events that have both M_L^{SJ25} and M_W^{Qopen} magnitude scales, there are 134 events with $M_L^{SJ25} \geq 2.5$, whereas 326 events meet the threshold of $M_W^{Qopen} \geq 2.5$ representing more than double the number of events. Future PHSA or physics-based studies in the Raton would benefit by taking into account: (1) the influence of b-values on seismic hazard forecasts and (2) the variability in earthquake rates depending on the magnitude threshold and scale used (e.g., M_L vs. M_W) when including small magnitude events.

Estimated b-values close to 1 have been found in some wastewater injection seismicity regions including northern Oklahoma (Cochran et al., 2020b), southern Kansas (Rubinstein et al., 2018), Guy–Greenbrier (Arkansas; Mousavi et al., 2017), the Sichuan Basin (China; Lei et al., 2019), and previously in the Raton Basin using local magnitudes (Wang et al., 2020b; Glasgow et al., 2021; Jamalreyhani et al., 2025). In contrast, we obtained b-values in the 1.2–1.4 range, which is higher than the commonly observed $b \approx 1$ in tectonic settings. Moreover, $b \approx 1$ in conjunction with other statistical analysis, such as nearest-neighbour distances (Zaliapin and Ben-Zion, 2013a,b), Epidemic Type Aftershock-Sequence models (Ogata, 1988), and interevent time distributions (Kagan and Jackson, 1991), has been interpreted as an indicator that the seismicity in the Raton Basin (Glasgow et al., 2021; Wang et al., 2020b) mimics tectonic settings (i.e., produces fewer background events and more clustered events). We do not attempt to reproduce all those analyses with the new b-values, but we expect that the higher b-values might indicate that some of the seismicity in the Raton Basin might deviate from the statistical behaviour of regular tectonic settings.

Another key factor in b-value estimation is the number of events available in the earthquake catalog. Recently, detection techniques including machine-learning (ML) earthquake phase detectors (Mousavi et al., 2020; Zhu and Beroza, 2018) have enabled increases in the number of earthquakes detected on a seismic network by about an order of magnitude. Most machine-learning based earthquake catalogs report local magnitudes because the calculation is integrated in several workflows (Zhang et al., 2022; Zhu et al., 2022). Future studies would benefit from implementing methods to estimate M_W when possible, as this would provide more accurate earthquake magnitudes. There are several potential methods and open codes available to estimate M_W for small events. Here, we just mention some of them and discuss their strengths and limitations: (i) SourceSpec (Satriano, 2022) (ii) Qopen (Eulenfeld et al., 2021), (iii) The Coda Calibration Tool CCT (Barno, 2017) or (iv) generalized inversion technique (Shible et al., 2022; Morasca et al., 2025). All of them are generally limited by the signal-to-noise ratio (SNR) in the time windows around the phase arrivals or the coda duration. The seismic network geometry and the source radiation pattern have large influences on M_W obtained with spectra from direct waves (Daniel, 2014). On the other hand, the coda methods (i.e., Qopen or CCT) are less sensitive to the radiation pattern (Mayeda et al., 2003). However, they require a high SNR for the entire coda duration, which might result in the exclusion of multiple events from an earthquake catalog. Moreover, some assumptions underlying each of the coda methods may not always be valid. The CCT method assumes an apparent stress value, which is usually unknown for earthquakes in many regions, to constrain the high-frequency part of the spectrum. Appar-

[1] We excluded one event as the closest 'Did you feel it?' report is from a distance > 200 km. https://earthquake.usgs.gov/earthquakes/eventpage/us1000jaq1/dyfi/intensity-vs-distance,

ent stress values might be obtained with a companion software of the CCT, named Coda Envelope Ratio Tool (CERT, based on Walter et al., 2017). Patton et al. (2025) show that, when the apparent stresses of the calibration earthquakes are unknown, selecting different assumed apparent stress values in the CCT methods affects the estimated M_W for events with $M < 3$. Moreover, the CCT method requires a set of events with well-calibrated M_W from other methods such as MT inversions. The Qopen method has the advantage of using a physical model of the scattering process, but the attenuation parameters represent average values of the entire crustal layer (Eulenfeld and Wegler, 2016). The GIT method can disentangle the source spectra, attenuation, and site amplification effects, but it seems more robust to obtain a site response factor in comparison to source and attenuation terms (Shible et al., 2022). Additionally, the GIT method requires testing the optimal inversion scheme on each dataset (parametric or non-parametric). We provide links to each of these methods in the Data and Resources section.

5 Conclusions

We applied a coda envelope fitting method (i.e., Qopen) (Eulenfeld et al., 2021) and estimated the moment magnitudes M_W for 31,581 earthquakes in the Raton Basin (Figure 1). We compare our M_W estimates with those from a previous study (Jamalreyhani et al., 2025) and events reported in ComCat and find that local magnitudes underestimate the size of the events relative to moment magnitudes (Figure 3). Linear relationships were developed between M_W and other local magnitudes that could be used in future studies in the Raton Basin. The M_W^{Qopen} results agree well with M_W estimates from moment tensor inversions and those reported in ComCat. Extending the use of M_W to smaller magnitudes with Qopen coda envelope fitting provides a different perspective on basic earthquake statistics in the Raton Basin. The derived frequency–magnitude relationship b-values using the M_W scale are 1.2–1.4, in contrast to $\approx$ 1 for M_L scales. The magnitude of completeness also increases from 0.7 to 1.3 when we change the magnitude scale from M_L to M_W. Other seismically active regions might have different b-values and M_C if they are calculated with local magnitudes rather than M_W. The results suggest that broader use of the coda envelope M_W for low-magnitude earthquakes could provide new perspectives on earthquake statistics and better facilitate comparison across localities.

Data and Resources

Waveform data and metadata used in this study are publicly available through the Incorporated Research Institutions for Seismology Data Management Center (IRIS DMC; http://ds.iris.edu/ds/nodes/dmc/). The seismic networks are: TA (https://doi.org/10.7914/SN/TA), C0 (https://doi.org/10.7914/SN/C0), and YX (https://doi.org/10.7914/SN/YX_2016). Additional data processing and plotting were performed using ObsPy (Beyreuther et al., 2010), NumPy (Harris et al., 2020), pandas (The pandas development team, 2020), PyGMT (Tian et al., 2023) (a Python wrapper for the Generic Mapping Tools; Wessel et al., 2019), and Matplotlib (Hunter, 2007). Methods to estimate M_W are available in the following links: SourceSpec (https://github.com/SeismicSource/sourcespec), CCT (https://github.com/LLNL/coda-calibration-tool) and its companion CERT (https://www.osti.gov/biblio/code-105734), Qopen (https://github.com/trichter/qopen), and GIT (Python version: GitPy, https://gitlab.rm.ingv.it/inversion/gitpy).

Acknowledgements

This research was supported by U.S. Geological Survey EHP Grant G24AP00218. Private landowners, including the Vermejo Park Ranch, generously hosted seismometers. We thank David Shelly, two anonymous reviewers, and Seismica editor Giuseppe Petrillo for insightful comments that improved the content of this study. Any use of trade, firm, or product names is for descriptive purposes and does not imply endorsement by the U.S. Government.

Competing interests

The authors declare no conflict of interest relevant to this study.

References

Abercrombie, R. E. Earthquake source scaling relationships from -1 to 5 M_L using seismograms recorded at 2.5-km depth. *Journal of Geophysical Research: Solid Earth*, 100(B12):24015–24036, Dec. 1995. doi: 10.1029/95jb02397.

Aki, K. Maximum likelihood estimate of b in the formula log N= a-bM and its confidence limits. *Bull. Earthquake Res. Inst., Tokyo Univ.*, 43:237–239, 1965.

Alvizuri, C. and Tape, C. Full moment tensors for small events (M_W< 3) at Uturuncu volcano, Bolivia. *Geophysical Journal International*, 206(3):1761–1783, July 2016. doi: 10.1093/gji/ggw247.

Amorese, D. Applying a Change-Point Detection Method on Frequency-Magnitude Distributions. *Bulletin of the Seismological Society of America*, 97(5):1742–1749, Oct. 2007. doi: 10.1785/0120060181.

Andrews, D. J. *Objective Determination of Source Parameters and Similarity of Earthquakes of Different Size*, page 259–267. American Geophysical Union, Mar. 2013. doi: 10.1029/gm037p0259.

Archuleta, R. J., Cranswick, E., Mueller, C., and Spudich, P. Source parameters of the 1980 Mammoth Lakes, California, earthquake sequence. *Journal of Geophysical Research: Solid Earth*, 87(B6): 4595–4607, June 1982. doi: 10.1029/jb087ib06p04595.

Bachmann, C. E., Wiemer, S., Goertz-Allmann, B. P., and Woessner, J. Influence of pore-pressure on the event-size distribution of induced earthquakes. *Geophysical Research Letters*, 39(9), May 2012. doi: 10.1029/2012gl051480.

Bakun, W. H. Seismic moments, local magnitudes, and coda-duration magnitudes for earthquakes in central California. *Bulletin of the Seismological Society of America*, 74(2):439–458, Apr. 1984. doi: 10.1785/bssa0740020439.

Bakun, W. H. and Joyner, W. B. The M_L scale in central California. *Bulletin of the Seismological Society of America*, 74(5): 1827–1843, Oct. 1984. doi: 10.1785/bssa0740051827.

Baltay, A. and Abercrombie, R. E. Seismic Moment and Local Magnitude Scales in Ridgecrest, California, from the SCEC/USGS Community Stress Drop Validation Study. *Bulletin of the Seismological Society of America*, 115(3):1279–1293, Apr. 2025. doi: 10.1785/0120240162.

Baltay, A., Abercrombie, R., Chu, S., and Taira, T. The SCEC/USGS Community Stress Drop Validation Study Using the 2019 Ridgecrest Earthquake Sequence. *Seismica*, 3(1), May 2024. doi: 10.26443/seismica.v3i1.1009.

Barnhart, W. D., Benz, H. M., Hayes, G. P., Rubinstein, J. L., and Bergman, E. Seismological and geodetic constraints on the 2011 Mw 5.3 Trinidad, Colorado earthquake and induced deformation in the Raton Basin. *Journal of Geophysical Research: Solid Earth*, 119(10):7923–7933, Oct. 2014. doi: 10.1002/2014jb011227.

Barno, J. LLNL/coda-calibration-tool. [Computer Software] https://doi.org/10.11578/dc.20180306.1, dec 2017. doi: 10.11578/dc.20180306.1. Tool for calibrating 1D coda seismic models.

Ben-Zion, Y. On quantification of the earthquake source. *Seismological Research Letters*, 72(2):151–152, 2001.

Ben-Zion, Y. and Zhu, L. Potency-magnitude scaling relations for southern California earthquakes with $1.0 < M_L < 7.0$. *Geophysical Journal International*, 148(3):F1–F5, Mar. 2002. doi: 10.1046/j.1365-246x.2002.01637.x.

Bender, B. Maximum likelihood estimation of b values for magnitude grouped data. *Bulletin of the Seismological Society of America*, 73(3):831–851, June 1983. doi: 10.1785/bssa0730030831.

Benz, H. M., McMahon, N. D., Aster, R. C., McNamara, D. E., and Harris, D. B. Hundreds of Earthquakes per Day: The 2014 Guthrie, Oklahoma, Earthquake Sequence. *Seismological Research Letters*, 86(5):1318–1325, July 2015. doi: 10.1785/0220150019.

Bethmann, F., Deichmann, N., and Mai, P. M. Scaling Relations of Local Magnitude versus Moment Magnitude for Sequences of Similar Earthquakes in Switzerland. *Bulletin of the Seismological Society of America*, 101(2):515–534, Mar. 2011. doi: 10.1785/0120100179.

Beyreuther, M., Barsch, R., Krischer, L., Megies, T., Behr, Y., and Wassermann, J. ObsPy: A Python toolbox for seismology. *Seismological Research Letters*, 81(3):530–533, 2010. doi: 10.1785/gssrl.81.3.530.

Bindi, D., Zaccarelli, R., and Kotha, S. R. Local and Moment Magnitude Analysis in the Ridgecrest Region, California: Impact on Interevent Ground-Motion Variability. *Bulletin of the Seismological Society of America*, 111(1):339–355, Dec. 2020. doi: 10.1785/0120200227.

Cao, A. and Gao, S. S. Temporal variation of seismic b-values beneath northeastern Japan island arc. *Geophysical Research Letters*, 29(9), May 2002. doi: 10.1029/2001gl013775.

Castellaro, S. and Bormann, P. Performance of Different Regression Procedures on the Magnitude Conversion Problem. *Bulletin of the Seismological Society of America*, 97(4):1167–1175, Aug. 2007. doi: 10.1785/0120060102.

Castellaro, S., Mulargia, F., and Kagan, Y. Y. Regression problems for magnitudes. *Geophysical Journal International*, 165(3):913–930, June 2006. doi: 10.1111/j.1365-246x.2006.02955.x.

Castro, R., Anderson, J., and Singh, S. Site response, attenuation and source spectra of S waves along the Guerrero, Mexico, subduction zone. *Bulletin of the Seismological Society of America*, 80(6A):1481–1503, 1990.

Chovanová, Z. and Kristek, J. A Local Magnitude Scale for Slovakia, Central Europe. *Bulletin of the Seismological Society of America*, 108(5A):2756–2763, Sept. 2018. doi: 10.1785/0120180059.

Cochran, E. S., Skoumal, R. J., McPhillips, D., Ross, Z. E., and Keranen, K. M. Activation of optimally and unfavourably oriented faults in a uniform local stress field during the 2011 Prague, Oklahoma, sequence. *Geophysical Journal International*, 222(1): 153–168, Mar. 2020a. doi: 10.1093/gji/ggaa153.

Cochran, E. S., Wickham-Piotrowski, A., Kemna, K. B., Harrington, R. M., Dougherty, S. L., and Peña Castro, A. F. Minimal Clustering of Injection-Induced Earthquakes Observed with a Large-n Seismic Array. *Bulletin of the Seismological Society of America*, 110(5):2005–2017, May 2020b. doi: 10.1785/0120200101.

Cochran, E. S., Baltay, A., Chu, S., Abercrombie, R. E., Bindi, D., Chen, X., Parker, G. A., Pennington, C., Shearer, P. M., and Trugman, D. T. SCEC/USGS Community Stress-Drop Validation Study: How Spectral Fitting Approaches Influence Measured Source Parameters. *Bulletin of the Seismological Society of America*, 115(3):760–776, Dec. 2024a. doi: 10.1785/0120240140.

Cochran, E. S., Rubinstein, J. L., Barbour, A. J., and Kaven, J. O. Induced Seismicity Strategic Vision. USGS Circular 1509, U.S. Geological Survey, 2024b. doi: 10.3133/cir1509.

Dahm, T., Kühn, D., Cesca, S., Isken, M., and Heimann, S. Earthquake Moment Magnitudes from Peak Ground Displacements and Synthetic Green's Functions. *Seismica*, 3(2), Dec. 2024. doi: 10.26443/seismica.v3i2.1205.

Daniel, G. Bias in magnitude for earthquakes with unknown focal mechanism. *Geophysical Prospecting*, 62(4):848–861, May 2014. doi: 10.1111/1365-2478.12142.

Deichmann, N. Local Magnitude, a Moment Revisited. *Bulletin of the Seismological Society of America*, 96(4A):1267–1277, Aug. 2006. doi: 10.1785/0120050115.

Deichmann, N. Theoretical basis for the observed break in M_L/M_W scaling between small and large earthquakes. *Bulletin of the Seismological Society of America*, 107(2):505–520, Feb. 2017. doi: 10.1785/0120160318.

Di Bona, M. A Local Magnitude Scale for Crustal Earthquakes in Italy. *Bulletin of the Seismological Society of America*, 106(1): 242–258, Jan. 2016. doi: 10.1785/0120150155.

Dost, B., Edwards, B., and Bommer, J. J. The relationship between M and M_L: A review and application to induced seismicity in the Groningen Gas Field, The Netherlands. *Seismological Research Letters*, 89(3):1062–1074, Mar. 2018. doi: 10.1785/02201700247.

Dreger, D. S. *85.11 TDMT_INV: Time domain seismic moment tensor INVersion*, volume 81 of *International Geophysics*, page 1627. Academic Press, 2003. doi: 10.1016/S0074-6142(03)80290-5.

Edwards, B., Allmann, B., Fäh, D., and Clinton, J. Automatic computation of moment magnitudes for small earthquakes and the scaling of local to moment magnitude. *Geophysical Journal International*, 183(1):407–420, Aug. 2010. doi: 10.1111/j.1365-246x.2010.04743.x.

Eken, T. Moment magnitude estimates for central Anatolian earthquakes using coda waves. *Solid Earth*, 10(3):713–723, May 2019. doi: 10.5194/se-10-713-2019.

El-Isa, Z. and Eaton, D. W. Spatiotemporal variations in the b-value of earthquake magnitude–frequency distributions: Classification and causes. *Tectonophysics*, 615–616:1–11, Mar. 2014. doi: 10.1016/j.tecto.2013.12.001.

El-Isa, Z. H. Continuous-cyclic variations in the b-value of the earthquake frequency-magnitude distribution. *Earthquake Science*, 26(5):301–320, Oct. 2013. doi: 10.1007/s11589-013-0037-9.

Ellsworth, W. L. Injection-Induced Earthquakes. *Science*, 341

(6142), July 2013. doi: 10.1126/science.1225942.

Eulenfeld, T. and Wegler, U. Measurement of intrinsic and scattering attenuation of shear waves in two sedimentary basins and comparison to crystalline sites in Germany. *Geophysical Journal International*, 205(2):744–757, Mar. 2016. doi: 10.1093/gji/ggw035.

Eulenfeld, T. and Wegler, U. Crustal intrinsic and scattering attenuation of high-frequency shear waves in the contiguous United States. *Journal of Geophysical Research: Solid Earth*, 122(6): 4676–4690, June 2017. doi: 10.1002/2017jb014038.

Eulenfeld, T., Dahm, T., Heimann, S., and Wegler, U. Fast and Robust Earthquake Source Spectra and Moment Magnitudes from Envelope Inversion. *Bulletin of the Seismological Society of America*, 112(2):878–893, Nov. 2021. doi: 10.1785/0120210200.

Eulenfeld, T., Hillers, G., Vuorinen, T. A. T., and Wegler, U. Induced Earthquake Source Parameters, Attenuation, and Site Effects From Waveform Envelopes in the Fennoscandian Shield. *Journal of Geophysical Research: Solid Earth*, 128(4), Apr. 2023. doi: 10.1029/2022jb025162.

Frohlich, C. and Davis, S. D. Teleseismic b values; Or, much ado about 1.0. *Journal of Geophysical Research: Solid Earth*, 98(B1): 631–644, Jan. 1993. doi: 10.1029/92jb01891.

Gable, S. L. and Huang, Y. New Estimates of Magnitude-Frequency Distribution and *b*-Value Using Relative Magnitudes for the 2011 Prague, Oklahoma Earthquake Sequence. *Journal of Geophysical Research: Solid Earth*, 129(1):e2023JB026455, 2024. doi: 10.1029/2023JB026455.

Geffers, G.-M., Main, I. G., and Naylor, M. Biases in estimating b-values from small earthquake catalogues: how high are high b-values? *Geophysical Journal International*, 229(3):1840–1855, Jan. 2022. doi: 10.1093/gji/ggac028.

Glasgow, M. E., Schmandt, B., Wang, R., Zhang, M., Bilek, S. L., and Kiser, E. Raton Basin induced seismicity is hosted by networks of short basement faults and mimics tectonic earthquake statistics. *Journal of Geophysical Research: Solid Earth*, 126(11): e2021JB022839, 2021. doi: 10.1029/2021JB022839.

Godano, C. A new method for the estimation of the completeness magnitude. *Physics of the Earth and Planetary Interiors*, 263: 7–11, Feb. 2017. doi: 10.1016/j.pepi.2016.12.003.

Godano, C., Petrillo, G., and Lippiello, E. Evaluating the incompleteness magnitude using an unbiased estimate of the b value. *Geophysical Journal International*, 236(2):994–1001, 2024a. doi: 10.1093/gji/ggad466.

Godano, C., Tramelli, A., Petrillo, G., and Convertito, V. Testing the Predictive Power of b Value for Italian Seismicity. *Seismica*, 3(1), Feb. 2024b. doi: 10.26443/seismica.v3i1.1084.

Goebel, T. H. W., Schorlemmer, D., Becker, T. W., Dresen, G., and Sammis, C. G. Acoustic emissions document stress changes over many seismic cycles in stick-slip experiments. *Geophysical Research Letters*, 40(10):2049–2054, May 2013. doi: 10.1002/grl.50507.

Gong, J., Fan, W., and Parnell-Turner, R. Machine learning-based new earthquake catalog illuminates on-fault and off-fault seismicity patterns at the Discovery Transform Fault, East Pacific Rise. *Geochemistry, Geophysics, Geosystems*, 24(9), Sept. 2023. doi: 10.1029/2023gc011043.

Gutenberg, B. and Richter, C. F. Earthquake magnitude, intensity, energy, and acceleration (Second paper). *Bulletin of the Seismological Society of America*, 46(2):105–145, Apr. 1956. doi: 10.1785/bssa0460020105.

Hanks, T. C. and Boore, D. M. Moment-magnitude relations in theory and practice. *Journal of Geophysical Research: Solid Earth*, 89(B7):6229–6235, July 1984. doi: 10.1029/jb089ib07p06229.

Hanks, T. C. and Kanamori, H. A moment magnitude scale. *Journal of Geophysical Research: Solid Earth*, 84(B5):2348–2350, May 1979. doi: 10.1029/jb084ib05p02348.

Harris, C. R., Millman, K. J., Van Der Walt, S. J., Gommers, R., Virtanen, P., Cournapeau, D., Wieser, E., Taylor, J., Berg, S., Smith, N. J., et al. Array programming with NumPy. *Nature*, 585(7825): 357–362, 2020.

Heimann, S., Isken, M., Kühn, D., Sudhaus, H., Steinberg, A., Daout, S., Cesca, S., Bathke, H., and Dahm, T. Grond: A probabilistic earthquake source inversion framework, V1.0, 2018. doi: 10.5880/GFZ.2.1.2018.003.

Hill, R. G., Weingarten, M., Langenbruch, C., and Fialko, Y. Mitigation and optimization of induced seismicity using physics-based forecasting. *Journal of Geophysical Research: Solid Earth*, 129(11), Oct. 2024. doi: 10.1029/2024jb028759.

Holt, J., Whidden, K. M., Koper, K. D., Pankow, K. L., Mayeda, K., Pechmann, J. C., Edwards, B., Gök, R., and Walter, W. R. Toward robust and routine determination of Mw for small earthquakes: Application to the 2020 Mw 5.7 Magna, Utah, seismic sequence. *Seismological Research Letters*, 92(2A):725–740, Jan. 2021. doi: 10.1785/0220200320.

Hunter, J. D. Matplotlib: A 2D Graphics Environment. *Computing in Science & Engineering*, 9(3):90–95, 2007. doi: 10.1109/mcse.2007.55.

Hutton, L. K. and Boore, D. M. The M_L scale in southern California. *Bulletin of the Seismological Society of America*, 77(6): 2074–2094, Dec. 1987. doi: 10.1785/bssa0770062074.

Ibáñez, J. M., De Angelis, S., Díaz-Moreno, A., Hernández, P., Alguacil, G., Posadas, A., and Pérez, N. Insights into the 2011-2012 submarine eruption off the coast of El Hierro (Canary Islands, Spain) from statistical analyses of earthquake activity. *Geophysical Journal International*, 191(2):659–670, Aug. 2012. doi: 10.1111/j.1365-246x.2012.05629.x.

Ichinose, G. A., Anderson, J. G., Smith, K. D., and Zeng, Y. Source Parameters of Eastern California and Western Nevada Earthquakes from Regional Moment Tensor Inversion. *Bulletin of the Seismological Society of America*, 93(1):61–84, Feb. 2003. doi: 10.1785/0120020063.

Izgi, G., Eken, T., Gaebler, P., Eulenfeld, T., and Taymaz, T. Crustal seismic attenuation parameters in the western region of the North Anatolian Fault Zone. *Journal of Geodynamics*, 134: 101694, Feb. 2020. doi: 10.1016/j.jog.2020.101694.

Jamalreyhani, M., Wang, R., Schmandt, B., Felipe Peña Castro, A., and Glasgow, M. E. Evidence for Fluid Pressurization of Fault Zones and Persistent Sensitivity to Injection Rate Beneath the Raton Basin. *Geophysical Research Letters*, 52(13), July 2025. doi: 10.1029/2025gl114675.

Jost, M. L., Büßelberg, T., Jost, Ö., and Harjes, H.-P. Source parameters of injection-induced microearthquakes at 9 km depth at the KTB Deep Drilling site, Germany. *Bulletin of the Seismological Society of America*, 88(3):815–832, June 1998. doi: 10.1785/bssa0880030815.

Joyner, W. B., Boore, D. M., and Porcella, R. L. Peak horizontal acceleration and velocity from strong motion records including records from the 1979 Imperial Valley, California, earthquake. Technical Report Open-File Report 81-365, U.S. Geological Survey, 1981. doi: 10.3133/ofr81365.

Kagan, Y. Y. and Jackson, D. D. Long-Term Earthquake Clustering. *Geophysical Journal International*, 104(1):117–134, Jan. 1991. doi: 10.1111/j.1365-246x.1991.tb02498.x.

Kemna, K. B., Peña Castro, A. F., Harrington, R. M., and Cochran, E. S. Using a large-n seismic array to explore the robustness of spectral estimations. *Geophysical Research Letters*, 47(21), Oct. 2020. doi: 10.1029/2020gl089342.

Kemna, K. B., Verdecchia, A., and Harrington, R. M. Spatiotemporal evolution of earthquake static stress drop values in the 2016–2017 central Italy seismic sequence. *Journal of Geophysical Research: Solid Earth*, 126(11), Nov. 2021. doi: 10.1029/2021jb022566.

Kim, S. K. and Park, M. A. The Local Magnitude Scale in the Korean Peninsula. *Pure and Applied Geophysics*, 162(5):875–889, May 2005. doi: 10.1007/s00024-004-2646-7.

Kozłowska, M., Brudzinski, M. R., Friberg, P., Skoumal, R. J., Baxter, N. D., and Currie, B. S. Maturity of nearby faults influences seismic hazard from hydraulic fracturing. *Proceedings of the National Academy of Sciences*, 115(8), Feb. 2018. doi: 10.1073/pnas.1715284115.

Kwiatek, G., Plenkers, K., Nakatani, M., Yabe, Y., and Dresen, G. Frequency-Magnitude Characteristics Down to Magnitude -4.4 for Induced Seismicity Recorded at Mponeng Gold Mine, South Africa. *Bulletin of the Seismological Society of America*, 100(3): 1165–1173, May 2010. doi: 10.1785/0120090277.

Kwiatek, G., Goebel, T. H. W., and Dresen, G. Seismic moment tensor and b value variations over successive seismic cycles in laboratory stick-slip experiments. *Geophysical Research Letters*, 41 (16):5838–5846, Aug. 2014. doi: 10.1002/2014gl060159.

Kwiatek, G., Martínez-Garzón, P., Dresen, G., Bohnhoff, M., Sone, H., and Hartline, C. Effects of long-term fluid injection on induced seismicity parameters and maximum magnitude in northwestern part of The Geysers geothermal field. *Journal of Geophysical Research: Solid Earth*, 120(10):7085–7101, Oct. 2015. doi: 10.1002/2015jb012362.

Kwiatek, G., Saarno, T., Ader, T., Bluemle, F., Bohnhoff, M., Chendorain, M., Dresen, G., Heikkinen, P., Kukkonen, I., Leary, P., Leonhardt, M., Malin, P., Martínez-Garzón, P., Passmore, K., Passmore, P., Valenzuela, S., and Wollin, C. Controlling fluid-induced seismicity during a 6.1-km-deep geothermal stimulation in Finland. *Science Advances*, 5(5), May 2019. doi: 10.1126/sciadv.aav7224.

Langenbruch, C. and Zoback, M. D. How will induced seismicity in Oklahoma respond to decreased saltwater injection rates? *Science advances*, 2(11):e1601542, 2016. doi: 10.1126/sciadv.1601542.

Langenbruch, C., Weingarten, M., and Zoback, M. D. Physics-based forecasting of man-made earthquake hazards in Oklahoma and Kansas. *Nature Communications*, 9(1), Sept. 2018. doi: 10.1038/s41467-018-06167-4.

Lei, X., Huang, D., Su, J., Jiang, G., Wang, X., Wang, H., Guo, X., and Fu, H. Fault reactivation and earthquakes with magnitudes of up to Mw4.7 induced by shale-gas hydraulic fracturing in Sichuan Basin, China. *Scientific Reports*, 7(1), Aug. 2017. doi: 10.1038/s41598-017-08557-y.

Lei, X., Wang, Z., and Su, J. Possible link between long-term and short-term water injections and earthquakes in salt mine and shale gas site in Changning, south Sichuan Basin, China. *Earth and Planetary Physics*, 3(6):510–525, 2019. doi: 10.26464/epp2019052.

Li, L. and Luo, G. Can we obtain reliable seismic b-values for real-time catalogues? *Geophysical Journal International*, 237(3): 1554–1566, 2024.

Li, L., Luo, G., and Liu, M. The K- M Slope: A Potential Supplement for b-Value. *Seismological Research Letters*, Mar. 2023. doi: 10.1785/0220220268.

Lippiello, E. and Petrillo, G. b-more-incomplete and b-more positive: Insights on a robust estimator of magnitude distribution. *Journal of Geophysical Research: Solid Earth*, 129(2): e2023JB027849, 2024. doi: 10.1029/2023JB027849.

Liu, M., Li, H., Li, L., Zhang, M., and Wang, W. Multistage Nucleation of the 2021 Yangbi MS 6.4 Earthquake, Yunnan, China and Its Foreshocks. *Journal of Geophysical Research: Solid Earth*, 127 (5), May 2022. doi: 10.1029/2022jb024091.

Lombardi, A. M. A normalized distance test for co-determining the completeness magnitude and b-value of earthquake catalogs. *Journal of Geophysical Research: Solid Earth*, 126(3), Mar. 2021. doi: 10.1029/2020jb021242.

Malagnini, L. and Munafò, I. On the Relationship between ML and Mw in a Broad Range: An Example from the Apennines, Italy. *Bulletin of the Seismological Society of America*, Jan. 2018. doi: 10.1785/0120170303.

Marzocchi, W., Spassiani, I., Stallone, A., and Taroni, M. How to be fooled searching for significant variations of the b-value. *Geophysical Journal International*, 220(3):1845–1856, Nov. 2019. doi: 10.1093/gji/ggz541.

Matsumoto, S., Iio, Y., Sakai, S., and Kato, A. Strength dependency of frequency–magnitude distribution in earthquakes and implications for stress state criticality. *Nature Communications*, 15 (1), June 2024. doi: 10.1038/s41467-024-49422-7.

Mayeda, K. and Walter, W. R. Moment, energy, stress drop, and source spectra of western United States earthquakes from regional coda envelopes. *Journal of Geophysical Research: Solid Earth*, 101(B5):11195–11208, May 1996. doi: 10.1029/96jb00112.

Mayeda, K., Hofstetter, A., O'Boyle, J. L., and Walter, W. R. Stable and Transportable Regional Magnitudes Based on Coda-Derived Moment-Rate Spectra. *Bulletin of the Seismological Society of America*, 93(1):224–239, Feb. 2003. doi: 10.1785/0120020020.

Mayeda, K., Bindi, D., Roman-Nieves, J., Morasca, P., Dreger, D., Ji, C., Taira, T., Archuleta, R., Walter, W. R., and Barno, J. Source-Scaling Comparison and Validation for Ridgecrest, California: Radiated Energy, Apparent Stress, and Mw Using the Coda Calibration Tool ($2.6 < M_W < 7.1$). *Bulletin of the Seismological Society of America*, 115(3):890–907, Nov. 2024. doi: 10.1785/0120240143.

McMahon, N. D., Aster, R. C., Yeck, W. L., McNamara, D. E., and Benz, H. M. Spatiotemporal evolution of the 2011 Prague, Oklahoma, aftershock sequence revealed using subspace detection and relocation. *Geophysical Research Letters*, 44(14):7149–7158, July 2017. doi: 10.1002/2017gl072944.

Mignan, A. and Woessner, J. Estimating the magnitude of completeness for earthquake catalogs. *Community online resource for statistical seismicity analysis*, pages 1–45, 2012.

Morasca, P., Bindi, D., Mayeda, K., Roman-Nieves, J., Barno, J., Walter, W. R., and Spallarossa, D. Source scaling comparison and validation in central Italy: Data intensive direct Swaves versus the sparse data coda envelope methodology. *Geophysical Journal International*, 231(3):1573–1590, July 2022. doi: 10.1093/gji/ggac268.

Morasca, P., D'Amico, M., Spallarossa, D., Bindi, D., Picozzi, M., Oth, A., and Pacor, F. GITpy: A Python Implementation of the Generalized Inversion Technique. *Seismological Research Letters*, 96 (6):3866–3879, July 2025. doi: 10.1785/0220250042.

Moratto, L., Saraò, A., and Priolo, E. Moment magnitude (M_W) estimation of weak seismicity in northeastern Italy. *Seismological Research Letters*, 88(6):1455–1464, Oct. 2017. doi: 10.1785/0220170063.

Mousavi, S. M., Ogwari, P. O., Horton, S. P., and Langston, C. A. Spatio-temporal evolution of frequency-magnitude distribution and seismogenic index during initiation of induced seismicity at Guy-Greenbrier, Arkansas. *Physics of the Earth and Planetary Interiors*, 267:53–66, June 2017. doi: 10.1016/j.pepi.2017.04.005.

Mousavi, S. M., Ellsworth, W. L., Zhu, W., Chuang, L. Y., and Beroza, G. C. Earthquake transformer—an attentive deep-learning model for simultaneous earthquake detection and phase picking. *Nature Communications*, 11(1), Aug. 2020. doi: 10.1038/s41467-020-17591-w.

Munafò, I., Malagnini, L., and Chiaraluce, L. On the relationship between M_W and M_L for small earthquakes. *Bulletin of the Seismological Society of America*, 106(5):2402–2408, Sept. 2016. doi: 10.1785/0120160130.

Nakai, J. S., Weingarten, M., Sheehan, A. F., Bilek, S. L., and Ge, S. A Possible Causative Mechanism of Raton Basin, New Mexico and Colorado Earthquakes Using Recent Seismicity Patterns and Pore Pressure Modeling. *Journal of Geophysical Research: Solid Earth*, 122(10):8051–8065, Oct. 2017. doi: 10.1002/2017jb014415.

Ogata, Y. Statistical Models for Earthquake Occurrences and Residual Analysis for Point Processes. *Journal of the American Statistical Association*, 83(401):9–27, Mar. 1988. doi: 10.1080/01621459.1988.10478560.

Ogata, Y. and Katsura, K. Analysis of temporal and spatial heterogeneity of magnitude frequency distribution inferred from earthquake catalogues. *Geophysical Journal International*, 113(3):727–738, June 1993. doi: 10.1111/j.1365-246x.1993.tb04663.x.

Ottemoller, L. and Sargeant, S. A local magnitude scale M_L for the United Kingdom. *Bulletin of the Seismological Society of America*, 103(5):2884–2893, Sept. 2013. doi: 10.1785/0120130085.

Paasschens, J. C. J. Solution of the time-dependent Boltzmann equation. *Physical Review E*, 56(1):1135–1141, July 1997. doi: 10.1103/physreve.56.1135.

Pang, G., Koper, K. D., Mesimeri, M., Pankow, K. L., Baker, B., Farrell, J., Holt, J., Hale, J. M., Roberson, P., Burlacu, R., et al. Seismic analysis of the 2020 Magna, Utah, earthquake sequence: Evidence for a listric Wasatch fault. *Geophysical Research Letters*, 47(18):e2020GL089798, 2020.

Patton, A. M., Pennington, C. N., Walter, W. R., and Trugman, D. T. Exploring Uncertainty in Moment Estimation for Small Earthquakes in Southern Nevada Using the Coda Envelope Method. *Bulletin of the Seismological Society of America*, 115(3): 1308–1317, Jan. 2025. doi: 10.1785/0120240120.

Petersen, M. D., Mueller, C. S., Moschetti, M. P., Hoover, S. M., Shumway, A. M., McNamara, D. E., Williams, R. A., Llenos, A. L., Ellsworth, W. L., Michael, A. J., Rubinstein, J. L., McGarr, A. F., and Rukstales, K. S. 2017 one-year seismic-hazard forecast for the central and eastern United States from induced and natural earthquakes. *Seismological Research Letters*, 88(3):772–783, Mar. 2017. doi: 10.1785/0220170005.

Petersen, M. D., Mueller, C. S., Moschetti, M. P., Hoover, S. M., Rukstales, K. S., McNamara, D. E., Williams, R. A., Shumway, A. M., Powers, P. M., Earle, P. S., Llenos, A. L., Michael, A. J., Rubinstein, J. L., Norbeck, J. H., and Cochran, E. S. 2018 one-year seismic hazard forecast for the central and eastern United States from induced and natural earthquakes. *Seismological Research Letters*, 89(3):1049–1061, Mar. 2018. doi: 10.1785/0220180005.

Pezzo, G., Billi, A., Carminati, E., Conti, A., De Gori, P., Devoti, R., Lucente, F. P., Palano, M., Petracchini, L., Serpelloni, E., Tavani, S., and Chiarabba, C. Seismic source identification of the 9 November 2022 Mw 5.5 offshore Adriatic sea (Italy) earthquake from GNSS data and aftershock relocation. *Scientific Reports*, 13(1), July 2023. doi: 10.1038/s41598-023-38150-5.

Prieto, G. A., Shearer, P. M., Vernon, F. L., and Kilb, D. Earthquake source scaling and self-similarity estimation from stacking P and S spectra. *Journal of Geophysical Research: Solid Earth*, 109 (B8), Aug. 2004. doi: 10.1029/2004jb003084.

Richter, C. F. An instrumental earthquake magnitude scale. *Bulletin of the Seismological Society of America*, 25(1):1–32, Jan. 1935. doi: 10.1785/bssa0250010001.

Ross, Z. E., Ben-Zion, Y., White, M. C., and Vernon, F. L. Analysis of earthquake body wave spectra for potency and magnitude values: implications for magnitude scaling relations. *Geophysical Journal International*, 207(2):1158–1164, Sept. 2016. doi: 10.1093/gji/ggw327.

Rubinstein, J. L., Ellsworth, W. L., McGarr, A., and Benz, H. M. The 2001–present induced earthquake sequence in the Raton Basin of northern New Mexico and southern Colorado. *Bulletin of the Seismological Society of America*, 104(5):2162–2181, Sept. 2014. doi: 10.1785/0120140009.

Rubinstein, J. L., Ellsworth, W. L., and Dougherty, S. L. The 2013–2016 induced earthquakes in Harper and Sumner Counties, southern Kansas. *Bulletin of the Seismological Society of America*, 108(2):674–689, Feb. 2018. doi: 10.1785/0120170209.

Sandri, L. and Marzocchi, W. A technical note on the bias in the estimation of the b-value and its uncertainty through the Least Squares technique. *Annals of Geophysics*, 50(3), Dec. 2007. doi: 10.4401/ag-4432.

Satriano, C. SourceSpec – Earthquake source parameters from P- or S-wave displacement spectra, 2022. doi: 10.5281/ZENODO.3688587.

Scherbaum, F. Combined inversion for the three-dimensional Q structure and source parameters using microearthquake spectra. *Journal of Geophysical Research: Solid Earth*, 95(B8): 12423–12438, Aug. 1990. doi: 10.1029/jb095ib08p12423.

Schorlemmer, D., Wiemer, S., and Wyss, M. Variations in earthquake-size distribution across different stress regimes. *Nature*, 437(7058):539–542, Sept. 2005. doi: 10.1038/nature04094.

Sens-Schönfelder, C. and Wegler, U. Radiative transfer theory for estimation of the seismic moment. *Geophysical Journal International*, 167(3):1363–1372, Dec. 2006. doi: 10.1111/j.1365-246x.2006.03139.x.

Shearer, P. M. *Introduction to Seismology*. Cambridge University Press, May 2019. doi: 10.1017/9781316877111.

Shelly, D. R., Ellsworth, W. L., and Hill, D. P. Fluid-faulting evolution in high definition: Connecting fault structure and frequency-magnitude variations during the 2014 Long Valley Caldera, California, earthquake swarm. *Journal of Geophysical Research: Solid Earth*, 121(3):1776–1795, Mar. 2016. doi: 10.1002/2015jb012719.

Shelly, D. R., Mayeda, K., Barno, J., Whidden, K. M., Moschetti, M. P., Llenos, A. L., Rubinstein, J. L., Yeck, W. L., Earle, P. S., Gök, R., and Walter, W. R. A big problem for small earthquakes: Benchmarking routine magnitudes and conversion relationships with coda envelope-derived M_W in southern Kansas and northern Oklahoma. *Bulletin of the Seismological Society of America*, 112(1): 210–225, Aug. 2021. doi: 10.1785/0120210115.

Shi, Y. and Bolt, B. A. The standard error of the magnitude-frequency b value. *Bulletin of the Seismological Society of America*, 72(5):1677–1687, Oct. 1982. doi: 10.1785/bssa0720051677.

Shible, H., Hollender, F., Bindi, D., Traversa, P., Oth, A., Edwards, B., Klin, P., Kawase, H., Grendas, I., Castro, R. R., Theodoulidis, N., and Gueguen, P. GITEC: A Generalized Inversion Technique Benchmark. *Bulletin of the Seismological Society of America*, 112 (2):850–877, Feb. 2022. doi: 10.1785/0120210242.

Skoumal, R. J., Brudzinski, M. R., Currie, B. S., and Ries, R. Temporal patterns of induced seismicity in Oklahoma revealed from multi-station template matching. *Journal of Seismology*, 24(5): 921–935, Aug. 2019. doi: 10.1007/s10950-019-09864-9.

Spassiani, I., Taroni, M., Murru, M., and Falcone, G. Real time Gutenberg–Richter b-value estimation for an ongoing seismic sequence: An application to the 2022 marche offshore earthquake sequence (M_L 5.7 central Italy). *Geophysical Journal International*, 234(2):1326–1331, Mar. 2023. doi: 10.1093/gji/ggad134.

Stokes, S. M., Ge, S., Brown, M. R. M., Menezes, E. A., Sheehan, A. F., and Tiampo, K. F. Pore Pressure Diffusion and Onset of Induced Seismicity. *Journal of Geophysical Research: Solid Earth*, 128(3), Feb. 2023. doi: 10.1029/2022jb026012.

Tan, Y. J., Waldhauser, F., Ellsworth, W. L., Zhang, M., Zhu, W., Michele, M., Chiaraluce, L., Beroza, G. C., and Segou, M. Machine-learning-based high-resolution earthquake catalog reveals how complex fault structures were activated during the 2016–2017 central Italy sequence. *The Seismic Record*, 1(1): 11–19, Apr. 2021. doi: 10.1785/0320210001.

Taroni, M. Estimating the Magnitude of Completeness of Earthquake Catalogs Using a Simple Random Variable Transformation. *The Seismic Record*, 3(3):194–199, July 2023. doi: 10.1785/0320230017.

Taroni, M. and Akinci, A. Good practices in PSHA: declustering, b-value estimation, foreshocks and aftershocks inclusion; a case study in Italy. *Geophysical Journal International*, 224(2): 1174–1187, Sept. 2020. doi: 10.1093/gji/ggaa462.

Teng, G. and Baker, J. W. Seismicity declustering and hazard analysis of the Oklahoma–Kansas region. *Bulletin of the Seismological Society of America*, 109(6):2356–2366, Oct. 2019. doi: 10.1785/0120190111.

Thapa, N., Dresen, G., and Goebel, T. H. W. Does b-value increase with pore-pressure?: Insights from laboratory experiments and induced seismicity. *Geophysical Research Letters*, 52 (11):e2025GL115740, 2025.

The pandas development team. pandas-dev/pandas: Pandas, Feb. 2020. doi: 10.5281/zenodo.3509134.

Tian, D., Uieda, L., Leong, W. J., Schlitzer, W., Fröhlich, Y., Grund, M., Jones, M., Toney, L., Yao, J., Magen, Y., Tong, J.-H., Materna, K., Belem, A., Newton, T., Anant, A., Ziebarth, M., Quinn, J., and Wessel, P. PyGMT: A Python interface for the Generic Mapping Tools, 2023. doi: 10.5281/ZENODO.8303186.

Trugman, D. T. Stress-Drop and Source Scaling of the 2019 Ridgecrest, California, Earthquake Sequence. *Bulletin of the Seismological Society of America*, 110(4):1859–1871, May 2020. doi: 10.1785/0120200009.

Trugman, D. T. and Ben-Zion, Y. Potency–magnitude scaling relations and a unified earthquake catalog for the Western United States. *The Seismic Record*, 4(3):223–230, July 2024. doi: 10.1785/0320240022.

U.S. Geological Survey Earthquake Hazards Program. Advanced National Seismic System (ANSS) Comprehensive Catalog of Earthquake Events and Products, 2025. https://earthquake.usgs.gov/earthquakes/search/. Accessed 30 May 2025.

Utsu, T. A Statistical Significance Test of the Difference in b-value between Two Earthquake Groups. *Journal of Physics of the Earth*, 14(2):37–40, 1966. doi: 10.4294/jpe1952.14.37.

Valensise, G., Console, R., Carluccio, R., and Vannoli, P. Seismotectonics-Driven Estimation of b-Value: Implications for Seismic Hazard Assessment. *Seismological Research Letters*, 95(6):3192–3206, June 2024. doi: 10.1785/0220240030.

van der Elst, N. J. B-positive: A robust estimator of aftershock magnitude distribution in transiently incomplete catalogs. *Journal of Geophysical Research: Solid Earth*, 126(2), Feb. 2021. doi: 10.1029/2020jb021027.

Verdon, J. P. and Bommer, J. J. Green, yellow, red, or out of the blue? An assessment of Traffic Light Schemes to mitigate the impact of hydraulic fracturing-induced seismicity. *Journal of Seismology*, 25(1):301–326, Oct. 2020. doi: 10.1007/s10950-020-09966-9.

Wald, D. J., Quitoriano, V., Worden, C. B., Hopper, M., and Dewey, J. W. USGS "Did You Feel It?" Internet-based macroseismic intensity maps. *Annals of Geophysics*, 54(6), Jan. 2012. doi: 10.4401/ag-5354.

Waldhauser, F. and Ellsworth, W. L. A double-difference earthquake location algorithm: Method and application to the northern Hayward fault, California. *Bulletin of the seismological society of America*, 90(6):1353–1368, 2000.

Walter, W. R., Yoo, S., Mayeda, K., and Gök, R. Earthquake stress via event ratio levels: Application to the 2011 and 2016 Oklahoma seismic sequences. *Geophysical Research Letters*, 44(7): 3147–3155, Apr. 2017. doi: 10.1002/2016gl072348.

Wang, B., Harrington, R. M., Liu, Y., Kao, H., and Yu, H. A Study on the Largest Hydraulic-Fracturing-Induced Earthquake in Canada: Observations and Static Stress-Drop Estimation. *Bulletin of the Seismological Society of America*, 110(5):2283–2294, July 2020a. doi: 10.1785/0120190261.

Wang, R., Schmandt, B., Zhang, M., Glasgow, M. E., Kiser, E., Rysanek, S., and Stairs, R. K. Injection-induced earthquakes on complex fault zones of the Raton Basin illuminated by machine-learning phase picker and dense nodal array. *Geophysical Research Letters*, 47:e2020GL088168, 2020b. doi: 10.1029/2020GL088168.

Wang, X., Li, J., Feng, A., and Sornette, D. Estimating magnitude completeness in earthquake catalogs: A comparative study of catalog-based methods. *Journal of Geophysical Research: Solid Earth*, 130(9), Sept. 2025. doi: 10.1029/2025jb031441.

Warren-Smith, E., Chamberlain, C. J., Lamb, S., and Townend, J. High-precision analysis of an aftershock sequence using matched-filter detection: The 4 May 2015 M_L 6 Wanaka earthquake, Southern Alps, New Zealand. *Seismological Research Letters*, 88(4):1065–1077, June 2017. doi: 10.1785/0220170016.

Wessel, P., Luis, J. F., Uieda, L., Scharroo, R., Wobbe, F., Smith, W. H. F., and Tian, D. The Generic Mapping Tools Version 6. *Geochemistry, Geophysics, Geosystems*, 20(11):5556–5564, Nov. 2019. doi: 10.1029/2019gc008515.

Wiemer, S. and Wyss, M. Minimum Magnitude of Completeness in Earthquake Catalogs: Examples from Alaska, the Western United States, and Japan. *Bulletin of the Seismological Society of America*, 90(4):859–869, Aug. 2000. doi: 10.1785/0119990114.

Wiens, D. A. Seismological constraints on the mechanism of deep earthquakes: temperature dependence of deep earthquake source properties. *Physics of the Earth and Planetary Interiors*, 127(1–4):145–163, Dec. 2001. doi: 10.1016/s0031-9201(01)00225-4.

Woessner, J. and Wiemer, S. Assessing the Quality of Earthquake Catalogues: Estimating the Magnitude of Completeness and Its Uncertainty. *Bulletin of the Seismological Society of America*, 95 (2):684–698, Apr. 2005. doi: 10.1785/0120040007.

Yenier, E. A Local Magnitude Relation for Earthquakes in the Western Canada Sedimentary Basin. *Bulletin of the Seismological Society of America*, 107(3):1421–1431, Apr. 2017. doi: 10.1785/0120160275.

Zaliapin, I. and Ben-Zion, Y. Earthquake clusters in southern California II: Classification and relation to physical properties of the crust. *Journal of Geophysical Research: Solid Earth*, 118(6): 2865–2877, June 2013a. doi: 10.1002/jgrb.50178.

Zaliapin, I. and Ben-Zion, Y. Earthquake clusters in southern California I: Identification and stability. *Journal of Geophysi-*

cal Research: Solid Earth, 118(6):2847–2864, June 2013b. doi: 10.1002/jgrb.50179.

Zhang, M., Ellsworth, W. L., and Beroza, G. C. Rapid Earthquake Association and Location. *Seismological Research Letters*, 90(6): 2276–2284, Sept. 2019. doi: 10.1785/0220190052.

Zhang, M., Liu, M., Feng, T., Wang, R., and Zhu, W. LOC-FLOW: An End-to-End Machine Learning-Based High-Precision Earthquake Location Workflow. *Seismological Research Letters*, 93(5): 2426–2438, Mar. 2022. doi: 10.1785/0220220019.

Zhou, Y., Zhou, S., and Zhuang, J. A test on methods for MC estimation based on earthquake catalog. *Earth and Planetary Physics*, 2(2):150–162, 2018.

Zhu, W. and Beroza, G. C. PhaseNet: A deep-neural-network-based seismic arrival-time picking method. *Geophysical Journal International*, Oct. 2018. doi: 10.1093/gji/ggy423.

Zhu, W., Hou, A. B., Yang, R., Datta, A., Mousavi, S. M., Ellsworth, W. L., and Beroza, G. C. QuakeFlow: a scalable machine-learning-based earthquake monitoring workflow with cloud computing. *Geophysical Journal International*, 232(1):684–693, Sept. 2022. doi: 10.1093/gji/ggac355.